Mechanistic Characterization of the HDV Genomic Ribozyme: Assessing the Catalytic and Structural Contributions of Divalent Metal Ions within a Multichannel Reaction Mechanism†

Shu-ichi Nakano,‡ David J. Proctor, and Philip C. Bevilacqua*

Department of Chemistry, The Pennsylvania State University, University Park, Pennsylvania 16802

Received June 18, 2001; Revised Manuscript Received July 31, 2001

ABSTRACT: Hepatitis delta virus (HDV) uses genomic and antigenomic ribozymes in its replication cycle. We examined ribozyme self-cleavage over eight orders of magnitude of Mg^{2+} concentration, from $\approx 10^{-9}$ to 10^{-1} M. These experiments were carried out in 1 M NaCl to aid folding of the ribozyme and to control the ionic strength. The concentration of free Mg^{2+} ions was established using an EDTA-Mg^{2+} buffered system. Over the pH range of 5−9, the rate was independent of Mg^{2+} concentration up to 10^{-7} M, and of the addition of a large excess of EDTA. This suggests that in the presence of 1 M NaCl, the ribozyme can fold and cleave without using divalent metal ions. Brønsted analysis under these reaction conditions suggests that solvent and hydroxide ions may play important roles as general base and specific base catalysts. The observed rate constant displayed a log-linear dependence on intermediate Mg^{2+} concentration from $\approx 10^{-7}$ to 10^{-4} M. These data combined with the shape of the pH profile under these conditions are consistent with the binding of at least one structural divalent metal ion that does not participate in catalysis and binds tighter at lower pH. No evidence for a catalytic role for Mg^{2+} was found at low or intermediate Mg^{2+} concentrations. Addition of Mg^{2+} to physiological and higher concentrations, from 10^{-3} to 10^{-1} M, revealed a second saturable divalent metal ion which binds tighter at high pH. The shape of the pH profile is inverted relative to that at low Mg^{2+} concentrations, consistent with a general acid−base catalysis mechanism in which a cytosine (C75) acts as the general acid and a hydroxide ion from the divalent metal ion, or possibly from solvent, acts as the base. Overall, the data support a model in which the HDV ribozyme can self-cleave by multiple divalent ion-independent and -dependent channels, and in which the contribution of Mg^{2+} to catalysis is modest at approximately 25-fold. Surface electrostatic potential maps were calculated on the self-cleaved form of the ribozyme using the nonlinear Poisson−Boltzmann equation. These calculations revealed several patches of high negative potential, one of which is present in a cleft near N4 of C75. These calculations suggest that distinct catalytic and structural metal ion sites exist on the ribozyme, and that the negative potential at the active site may help shift the pK_a for N3 of C75 toward neutrality.

The hepatitis delta virus (HDV)[1] ribozyme is a small, self-cleaving RNA that is responsible for processing nascent viral transcripts into unit-length monomers during replication (see Figure 1 for secondary and tertiary structures). The cleavage reaction leads to products with 5′-hydroxyl and 2′,3′-cyclic phosphate termini. A number of investigations of the cleavage mechanism have been performed (*1*−*3*), and a crystal structure of the self-cleaved form of the genomic ribozyme is available (*4*, *5*). The crystal structure shows the proximity of the N3 of cytosine 75 (C75) and the leaving group 5′-oxygen of G1. This formed part of the basis for a proposed mechanism in which C75 acts as a general acid to protonate the scissile P−O5′ bond in the transition state (*2*). In addition, reactivity−pH profiles and substitution of an adenine at position 75 revealed a pK_a near neutrality that can be assigned to C75. Negative linkage between proton binding to C75 and ribozyme binding of a catalytic Mg^{2+} supports protonation of C75 in the reactant state and a general acid role for C75 in bond cleavage (*2*). Similar experiments on the antigenomic ribozyme also demonstrated a pK_a near neutrality that can be assigned to C76 (C76 is the antigenomic counterpart to C75), and an inactive C76U mutant was rescued by imidazole, further supporting proton transfer by C75/76 (*1*).

† Supported in part by a fellowship from the Alfred P. Sloan Foundation and a Camille Dreyfus Teacher-Scholar Award to P.C.B.

* To whom correspondence should be addressed. Phone: (814) 863-3812. Fax: (814) 863-8403. E-mail: pcb@chem.psu.edu.

‡ Present address: High Technology Research Center, Konan University, 8-9-1 Okamoto, Higashinada-ku, Kobe 658-8501, Japan.

[1] Abbreviations: AS1(−30/−7), antisense oligomer complementary to nucleotides −30 to −7; C76, antigenomic counterpart to C75; EDTA, ethylenediaminetetraacetic acid; Hepes, 4-(2-hydroxyethyl)-1-piperazineethanesulfonic acid; G11C, ribozyme used in these studies with a G to C change at position 11; −30/99, G11C ribozyme beginning at position −30 and ending at position 99; HDV, hepatitis delta virus; MES, 2-(*N*-morpholino)ethanesulfonic acid; $[Mg(OH)]^+$ or $[Mg(H_2O)_5(OH)]^+$, hydrated magnesium hydroxide; NLPB, nonlinear Poisson−Boltzmann; TE, 10 mM Tris and 1 mM EDTA (pH 7.5); Tris, tris(hydroxymethyl)aminomethane; α_H, Hill constant; α, Brønsted coefficient for general acid catalysis; β, Brønsted coefficient for general base catalysis; K_a, observed acid dissociation constant; $K_{d,cat}$, observed dissociation constant for the catalytic Mg^{2+} ion; $K_{d,EDTA-Mg}$, conditional dissociation constant for all forms of uncomplexed EDTA and Mg^{2+}; $K_{d,MY}$, dissociation constant for Mg^{2+} and $EDTA^{4-}$; $K_{d,str}$, observed dissociation constant for the structural Mg^{2+} ion; k_i, observed cleavage rate constant for channel i; k_{obs}, observed rate constant for cleavage; kT/e, where k is the Boltzmann constant, T is the absolute temperature, and e is the charge on a proton.

10.1021/bi011253n CCC: $20.00
Published on Web 09/12/2001

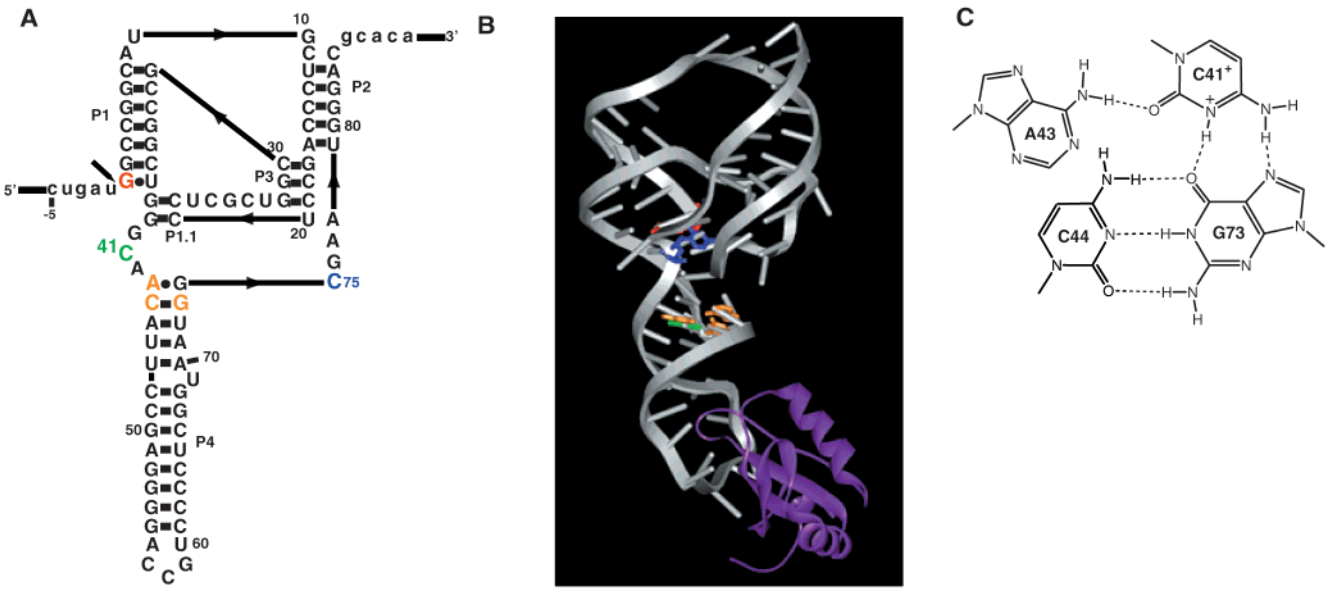

FIGURE 1: Various structures of the genomic HDV ribozyme. (A) Secondary structure of the HDV genomic ribozyme used in this study. The positions of bases relevant to the results are noted in color. The cleavage site between U−1 and G1 is denoted with an arrow. Flanking sequences are in lowercase and extend from position −30 to −1 and from position 85 to 99, as given elsewhere (*10*). Position 11 has a G to C change, which is a fast-folding variant that exhibits single-exponential cleavage kinetics (ref *2* and unpublished experiments of D. M. Chadalavada and P. C. Bevilacqua). (B) Crystal structure of the self-cleaved form of the ribozyme (*4*). Bases highlighted in the secondary structure are shown using the same colors. Also shown is the U1A protein which was used to facilitate crystallization (*4*). Drawn with WebLab ViewerLite (MSI). (C) Hydrogen bonding of the bases in the C41-containing base quartet. The distance of 2.9 Å between N3 of C41 and O6 of G73 suggests the existence of a hydrogen bond and therefore protonation of N3 (*5*).

The proposed mechanism also requires a general base with a pK_a of >9. One possibility is that hydrated magnesium hydroxide serves this role (*2*) since the pK_a for a water molecule coordinated to Mg^{2+} is 11.4 (*6*). However, the crystal structure does not provide evidence for well-ordered metal ions near the active site (*4*, *5*). Nevertheless, the absence of a bound magnesium ion in the structure does not rule out its participation in the reaction. For example, Mg^{2+} could require the scissile phosphate as a ligand or a cage to decrease its off-rate, Mg^{2+} could bind tightly only in the transition state, or the catalytic Mg^{2+} may be kinetically labile and not crystallize readily. Support for a bound metal ion at the cleavage site was also provided from a specificity switch of the reaction from Mg^{2+} or Ca^{2+} to Mg^{2+} only upon changing the cleavage site to a 2′−5′ linkage (*7*).

Despite the apparent involvement of a Mg^{2+} ion in the general base-catalyzed portion of the mechanism at the physiological salt conditions of ≈1 mM Mg^{2+} (*8*), at high ionic strengths the reaction can proceed in the absence of divalent metal ions (*2*). This result added the HDV ribozyme to the group that includes the hairpin, hammerhead, and VS1 ribozymes (*9*), those that are able to cleave in the absence of divalent metal ions. The ribozyme self-cleavage mechanism under such conditions remains enigmatic. Possible roles of solvent and hydroxide ion are poorly defined, and alternate roles of divalent metal ions in folding are unexplored in the HDV ribozyme.

To characterize the reaction further, we have carried out an extensive investigation of the Mg^{2+} dependence of the self-cleavage reaction of the genomic HDV ribozyme. The concentration of Mg^{2+} was tightly controlled by stringent treatment of the reagents with Chelex resin, and by titration of Mg^{2+} and EDTA over a large range of free Mg^{2+} concentrations in the presence of 1 M NaCl. Our data support binding of a noncatalytic divalent metal ion, or several ions, that leads to rate acceleration while maintaining the same pH dependence of the reaction without the catalytic divalent metal ion. The data also provide evidence for catalytic participation of solvent and hydroxide ions in the absence of a catalytic Mg^{2+} ion, and evidence that general base and specific base catalysis are important in the mechanism. These results are interpreted in the context of a mechanism in which the HDV ribozyme can self-cleave by a minimum of two divalent metal ion-independent and two divalent metal ion-dependent channels.

EXPERIMENTAL PROCEDURES

Materials

The −30/99 ribozyme was 5′-end-labeled with ^{32}P, and the reaction was initiated with saturating AS1(−30/−7) as described previously (*2*, *10*). A G11C change was present in all constructs, as this is a fast-folding ribozyme that reacts according to a single exponential (refs *2* and *10* and unpublished experiments of D. M. Chadalavada and P. C. Bevilacqua). NaCl (>99.0%) was purchased from VWR as 5 ppm heavy metals. HEPES (>99.0%) was from EM Science as RNase-free and <0.001% heavy metals, and MES (>99%) was from Sigma as RNase-free. To avoid precipitation of the EDTA at low pH, buffer/EDTA mixtures were prepared as 2× solutions immediately prior to use. The pH of a 0.25 M stock of buffer was determined using a glass electrode. The ionic strength of 0.5−1.0 M due to the presence of NaCl is expected to decrease the pK_a of these buffers by ∼0.16 unit (*11*). This correction is small relative to the error in the values of pK_a at high ionic strengths.

To help remove contaminating polyvalent metal ions from solutions, the metal-chelating resin Chelex 100 (Bio-Rad) was used. Chelex 100 is a resin of styrene divinylbenzene copolymers containing iminodiacetate anions. Approximately

0.25 g of the resin was poured into a column, and the sodium form of the resin was generated as described previously (*12*). All solutions except those containing divalent metal ions were passed through a Chelex column just before use. In particular, water, NaCl, EDTA/HEPES, and EDTA/MES mixtures were treated with Chelex. For low-EDTA concentration experiments, ribozyme and AS1(−30/−7) were placed in Eppendorf tubes into which a small amount of Chelex resin had been poured. The tubes were shaken, heated at 55 °C for 1 min to sequester polyvalent metal ions, and stored in the presence of a small amount of resin. In addition, all Eppendorf tubes were washed with Chelex-treated water prior to use.

Methods

To work at low concentrations of Mg^{2+}, it was necessary to use mixtures of $MgCl_2$ and EDTA. The first two methods sections describe steps necessary to perform these experiments.

Determination of $K_{d,EDTA-Mg}$ and $pK_{a,EDTA}$. The conditional dissociation constant, $K_{d,EDTA-Mg}$, is defined for the equilibrium between free Mg^{2+}, all ionization states of EDTA not complexed with Mg^{2+}, and the Mg^{2+}−$EDTA^{4-}$ complex (*13*); thus, $K_{d,EDTA-Mg}$ is a function of pH. Values for $K_{d,EDTA-Mg}$ at ionic strengths of up to 1 M NaCl were determined at 37 °C by the change in absorbance at 225 nm (ΔA_{225}) upon Mg^{2+} addition to 1 mM EDTA in the presence of 25 mM MES (pH 4.0−6.5) or 25 mM HEPES (pH 7.0 and 7.5). The absorbance of EDTA was measured in the far-UV region using a 0.5 cm cuvette and a Beckman DU 650 spectrophotometer. A wavelength of 225 nm was chosen because HEPES buffer shows a significant absorbance at $\lambda < 220$ nm. $K_{d,EDTA-Mg}$ was obtained from fitting to eq 1 for formation of the 1:1 Mg^{2+}−$EDTA^{4-}$ complex

$$\Delta A_{225} = \Delta A_{225,max}\{[([Mg^{2+}]_a + [E]_t + K_d) - \sqrt{([Mg^{2+}]_a + [E]_t + K_d)^2 - 4[Mg^{2+}]_a[E]_t}]/(2[E]_t)\} \quad (1)$$

where $\Delta A_{225,max}$ is the maximum absorbance change at 225 nm occurring upon saturation of the EDTA with Mg^{2+} and $[E]_t$ and $[Mg^{2+}]_a$ are the concentration of total EDTA and added Mg^{2+}, respectively. All curve fitting herein was achieved by a nonlinear least-squares method using KaleidaGraph (Synergy Software).

The values of $K_{d,EDTA-Mg}$ at pH 8.0 and 9.0 were too small to determine in the presence of contaminating polyvalent metal ions (see Results); therefore, $K_{d,EDTA-Mg}$ values were estimated using the relationship $K_{d,EDTA-Mg} = K_{d,MY}/\alpha^{4-}$ (*13*). $K_{d,MY}$ is the dissociation constant for Mg^{2+} and $EDTA^{4-}$, and is not a function of pH at pH values significantly below the pK_a of $Mg(H_2O)_6$ of 11.4. $\alpha^{4-} = [EDTA^{4-}]/[EDTA]$, where [EDTA] represents the concentration of all ionization states of EDTA not complexed with metal ion; α^{4-} is a function of pH and represents the fraction of EDTA that is functional for Mg^{2+} binding. Accordingly, the value of $K_{d,EDTA-Mg}$ could be estimated at high pH from the knowledge of α^{4-} and a plot of log $K_{d,EDTA-Mg}$ versus log α^{4-}. α^{4-} was calculated at a given pH according to eq 2

$$\alpha^{4-} = \frac{1}{1 + 10^{pK_{a4}-pH} + 10^{pK_{a3}+pK_{a4}-2pH}} \quad (2)$$

where pK_{a3} and pK_{a4} are defined for $K_{d,EDTA-Mg}$ as the transitions from the 2^- to 3^- and from the 3^- to 4^- species of EDTA, respectively. Terms involving pK_{a1} (≈2.0) and pK_{a2} (≈2.7) were omitted since the 1^- and neutral species of EDTA are not significantly populated at the pH values that were used (*14*). The values of pK_{a3} and pK_{a4} of EDTA were determined separately at various ionic strengths by monitoring the pH change upon addition of 10% HCl to a 10 mM EDTA solution (80 mL, initial pH of >11) at 37 °C. The pH value was monitored with a glass electrode that was calibrated about the EDTA pK_a of interest. The measured pH was fit to eq 3

$$Y = \frac{(a + c \times 10^{pH-pK_a})pH + (b + d \times 10^{pH-pK_a})}{1 + 10^{pH-pK_a}} \quad (3)$$

where *a* and *c* are the slopes and *b* and *d* are the intercepts of the acidic and basic baselines, respectively, and *Y* is the volume of HCl added. The value of pK_{a3} for EDTA was also estimated by monitoring the change in the extinction coefficient at 225 nm as a function of the amount of HCl added and fitting to an equation similar to eq 3.

Metal-Buffered System. To achieve reliable low concentrations of free Mg^{2+}, a metal-buffered system was used in which the majority of the Mg^{2+} was present as a complex with EDTA (*15*). In all cases, the concentrations of Mg^{2+} and EDTA were both in excess over that of the ribozyme. This approach allowed addition of Mg^{2+} in excess over the concentration of contaminating metal ion so that the total concentration of Mg^{2+} could be known reliably. An additional advantage is that EDTA binds most heavy metals tighter than Mg^{2+} (*13*), so working with EDTA−Mg^{2+} complexes ensures that any unidentified heavy metals are chelated. Since the estimated concentrations of the contaminating polyvalent metal ions were ≈2 μM (as Mg^{2+}) after treating the solutions with Chelex resin (see Results), the concentration of added Mg^{2+} was no less than 5 μM. In general, 1 mM EDTA was used, although 100 mM EDTA was necessary to generate low values of $[Mg^{2+}]_{uncomplexed}$ at pH 4.5, 5.0, and 6.0, and 0.1 mM EDTA was used to generate values of $[Mg^{2+}]_{uncomplexed}$ between 10^{-4} and 10^{-3} M at pH 7.0, 8.0, and 9.0. The concentration of uncomplexed Mg^{2+} was calculated using eq 4, where K_d represents $K_{d,EDTA-Mg}$.

$$[Mg^{2+}]_{uncomplexed} = [[Mg^{2+}]_a - [E]_t - K_d + \sqrt{([Mg^{2+}]_a + [E]_t + K_d)^2 - 4[Mg^{2+}]_a[E]_t}]/2 \quad (4)$$

Absorbance Titrations of Mg^{2+} Binding to Ribozyme. The changes in absorbance at 260 and 280 nm were determined upon titration of a 0.2 μM solution of the self-cleaved form of the ribozyme in 1 M NaCl and 25 mM HEPES (pH 7.0) with small volumes of the same solution also containing $MgCl_2$. The RNA was renatured by heating at 80 °C for 2 min before being used. The absorbance, *A*, was fit to eq 5

$$A = (a\ pMg + b) - \frac{(c\ pMg + d)}{1 + 10^{\alpha_H(pK_d - pMg)}} \quad (5)$$

where *a* and *b* are the slope and intercept of the low-pMg baseline, respectively, *c* and *d* are the differences in the slopes and intercepts of the low- and high-pMg baseline, respec-

Scheme 1

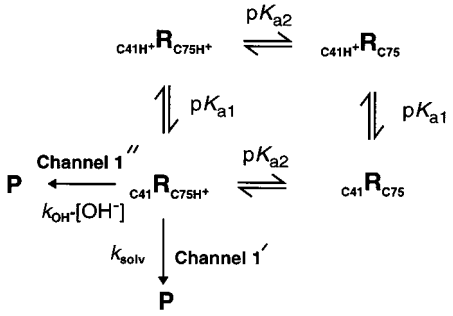

tively, α_H is the Hill constant, and K_d is the apparent dissociation constant. pMg was chosen as the *x*-axis to allow fitting to eq 5, which is similar to eq 3.

Kinetic Measurements. The 5′-end-labeled RNA was renatured at 55 °C for 10 min in TE and then kept at room temperature for 10 min. For low-EDTA concentration experiments, ribozyme and AS1(−30/−7) were treated with Chelex and were used as EDTA-free solutions. The antisense oligomer AS1(−30/−7) was added at a saturating concentration of 10 μM, followed by 25 mM MES (pH ≤6.5) or 25 mM HEPES (pH >6.5) containing variable concentrations of EDTA. (All concentrations are final.) The solution was incubated at 37 °C for 2 min, and a zero time point was removed. The cleavage reaction was initiated by addition of divalent ion, NaCl, or a divalent ion/NaCl mixture at 37 °C. All reagents were prewarmed at 37 °C, and the final RNA concentration was ∼0.3 nM. Aliquots were removed at known times, and the reaction was quenched by addition of an equal volume of a formamide solution containing EDTA (pH >10) at a concentration at least 2 times greater than the total divalent ion concentration. These aliquots were immediately frozen on powdered dry ice and stored at −20 °C until they were needed. Reaction mixtures were separated on a 10% polyacrylamide gel containing 7 M urea. Prior to electrophoresis, frozen samples were allowed to warm to room temperature but were not heated to avoid further reaction. The fraction RNA cleaved at each time point was quantitated on a PhosphorImager (Molecular Dynamics). Data were well fit by a single-exponential equation (eq 6)

$$f = A + B\exp(-k_{obs}t) \quad (6)$$

where f is fraction reaction and k_{obs} is the observed rate constant for the self-cleavage reaction. The reactions were single-exponential with no burst (i.e., $B \approx -A$) and proceeded to ≥80% completion. An initial rate approximation ($f = k_{obs}t$) was used to determine k_{obs} for slow reactions when completion was not reached.

Data Fitting for the Reactions without Divalent Ions. Reactivity−pH profiles were fit to eqs 7 and 8 to obtain pK_a values in the absence of the catalytic magnesium ion. The higher pK_a, pK_{a2} in Scheme 1, appears to be assignable to C75 (see Discussion). Equation 7 was derived from the kinetic model in Scheme 1 assuming only channel 1′, channel 1″, and pK_{a2} contribute.

$$k_{obs} = \frac{k_{solv} + k_{OH^-} \times 10^{pH-14}}{1 + 10^{pH-pK_{a2}}} \quad (7)$$

In this model, specific base catalysis by hydroxide ion is treated as being important at high pH as gauged by the plateau of the rate−pH profiles at high pH. k_{solv} is the rate constant for the solvent-catalyzed portion of the reaction (see Discussion), and k_{OH^-} is the rate constant for the specific base-catalyzed portion of the reaction. The second equation used to fit this set of data (eq 8) was derived from the entirety of the model in Scheme 1. The additional features for eq 8 are an inactive, doubly protonated state of the ribozyme, which occurs with a pK_{a1} (Scheme 1) that appears to be assignable to C41 (see Discussion), and a second singly protonated state in which C41 is protonated and C75 is unprotonated. This final term is significant only when ΔpK_a (=pK_{a2} − pK_{a1}) is small. The values of pK_{a1} and pK_{a2} were assumed to be independent of each other in the absence of data to suggest otherwise.

Scheme 2

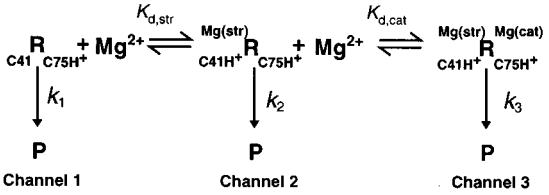

$$k_{obs} = \frac{k_{solv} + k_{OH^-} \times 10^{pH-14}}{1 + 10^{pK_{a1}-pH} + 10^{pH-pK_{a2}} + 10^{pK_{a1}-pK_{a2}}} \quad (8)$$

For both eqs 7 and 8, data were fit to log(k_{obs}), using the logarithm of eq 7 or 8.

Description and Data Fitting for the Multichannel Model. The dependence of log k_{obs} on Mg^{2+} concentration was described with the following set of equations. These were derived from Scheme 2 in which the ribozyme can self-cleave by three major channels separated by binding of structural and catalytic Mg^{2+} ions. Binding of structural and catalytic metal ions is depicted as ordered in the model in Scheme 2, since structural ions are presumably required for forming the catalytic site. This model is also supported by observed cooperative binding of metal ions at high pH (see Results and Discussion). It remains possible that the plateau behavior that is observed is caused by a change in the rate-limiting step at high Mg^{2+} concentrations rather than saturable metal ion binding; however, observation of multiple plateaus and cooperative Mg^{2+} binding under certain conditions (see Results) argues against this possibility. The species shown protonated in Scheme 2 for each channel are those believed to be the most rapid; however, each species is in equilibrium with a bank of two singly protonated states and a doubly unprotonated state, omitted for clarity. Channel 1 (Scheme 2) is really composed of two channels, channel 1′ and channel 1″ (Scheme 1); however, at constant pH, channel 1 can be modeled with a single rate constant k_1, where $k_1 = k_{obs}$ from eq 8. In addition, major channels 2 and 3 are also likely composed of additional channels. Channel 3 is assigned a rate constant of k_3, and the data are consistent with the relationship $k_3 \approx k_{[MgOH]^+} \times 10^{pK_{a,C75}-11.4}$, where $[Mg(OH)]^+$ represents $[Mg(H_2O)_5(OH)]^+$, $k_{[MgOH]^+}$ is the intrinsic rate constant in the presence of fully functional $[Mg(OH)]^+$, p$K_{a,C75}$ is the pK_a of C75, 11.4 is the pK_a of the hydrated Mg^{2+} ion, and $10^{pK_{a,C75}-11.4}$ is the fraction of ribozyme in the functional form in the plateau region of the pH profile. k_{obs}

Scheme 3

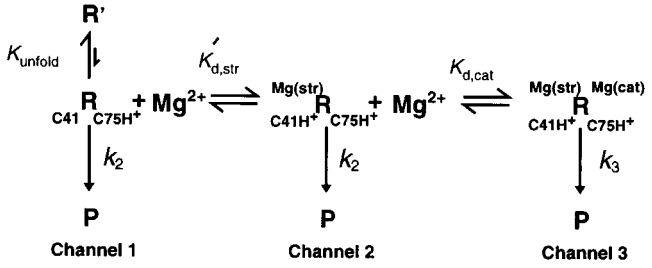

is the weighted sum of the rate constants for each channel

$$k_{obs} = k_1 f_1 + k_2 f_2 + k_3 f_3 \quad (9a)$$

where k_i is the rate constant for channel i and f_i is the fractional occupancy of channel i.

The fractional occupancies of each channel are as follows:

$$f_1 = \frac{K_{d,str}K_{d,cat}}{K_{d,str}K_{d,cat} + K_{d,cat}[Mg^{2+}] + [Mg^{2+}]^2} \quad (9b)$$

$$f_2 = \frac{K_{d,cat}[Mg^{2+}]}{K_{d,str}K_{d,cat} + K_{d,cat}[Mg^{2+}] + [Mg^{2+}]^2} \quad (9c)$$

$$f_3 = \frac{[Mg^{2+}]^2}{K_{d,str}K_{d,cat} + K_{d,cat}[Mg^{2+}] + [Mg^{2+}]^2} \quad (9d)$$

For a given pH, typically only a subset of the variables in eqs 9a−9d could be determined with confidence. Because of this complication, data were fit in one of two ways. Either log k_{obs} versus Mg^{2+} concentration was fit using the logarithm of eqs 9a−9d, or k_{obs} versus higher Mg^{2+} concentrations was fit to the Hill equation (eq 10) (*16*)

$$k_{obs} = \frac{k_{max}[Mg^{2+}]^{\alpha_H}/K_d^{\alpha_H}}{1 + [Mg^{2+}]^{\alpha_H}/K_d^{\alpha_H}} \quad (10)$$

where α_H is the Hill constant and K_d is the apparent dissociation constant. The Hill constant, α_H, gives a semiempirical index of cooperativity; if the binding of two Mg^{2+} ions is perfectly cooperative, then α_H is 2, and if no cooperativity occurs, α_H is 1. These ions could belong to the same or to different classes of metal binding sites.

An alternate multichannel mechanism is considered in Scheme 3, in which the ribozyme is assumed to form a significant amount of a cleavage-inactive conformer, R′. The equilibrium constant K_{unfold} is defined as [R′]/[R]. The observed values of k_1 and $K_{d,str}$ are related to their intrinsic values, k_2 (shown for channels 1 and 2 in Scheme 3) and $K'_{d,str}$ by the relationships

$$k_2 = k_1(1 + K_{unfold}) \quad (11)$$

$$K'_{d,str} = K_{d,str}/(1 + K_{unfold}) \quad (12)$$

Limiting Values of the Multichannel Model. To determine the value of k_1, the logarithm of eqs 9a−9d was used and the low Mg^{2+} concentration limit was taken (eq 13a). In these limits, the symbols "≪" and "≫" mean approximately 10-fold different. Each plot of log k_{obs} versus Mg^{2+} concentration had a Mg^{2+} concentration-independent portion that allowed k_1 to be determined.

$$\log k_{obs} \approx \log\left(k_1 + k_2\frac{[Mg^{2+}]}{K_{d,str}} + k_3\frac{[Mg^{2+}]^2}{K_{d,str}K_{d,cat}}\right) \quad [Mg^{2+}] \ll K_{d,str} \text{ and } K_{d,cat} \quad (13a)$$

At subsaturating but somewhat higher Mg^{2+} concentrations, the order of the reaction with respect to Mg^{2+} concentration is of interest. For conditions in which $[Mg^{2+}] < K_{d,str} < K_{d,cat}$, and $K_{d,str}(k_1/k_2) \ll [Mg^{2+}] \ll K_{d,cat}(k_2/k_3)$, eqs 9a−9d reduce to eq 13b

$$\log k_{obs} \approx \log[Mg^{2+}] + \log\frac{k_2}{K_{d,str}} \quad (13b)$$

and the slope of a log k_{obs}−log$[Mg^{2+}]$ plot should be unity, representing binding of the structural metal ion and occupancy of channel 2.

On the other hand, if $[Mg^{2+}] < K_{d,cat} < K_{d,str}$, then two portions of the Mg^{2+}-dependent plot need be considered. Under conditions in which $K_{d,cat}(k_2/k_3) \ll [Mg^{2+}] \ll K_{d,str}$, eqs 9a−9d reduce to eq 13c

$$\log k_{obs} \approx 2(\log[Mg^{2+}]) + \log[k_3/(K_{d,str}K_{d,cat})] \quad (13c)$$

and the slope of a log k_{obs}−log$[Mg^{2+}]$ plot should approach 2, representing cooperative binding of the structural and catalytic metal ions and occupancy of channel 3. However, under conditions in which $[Mg^{2+}] < K_{d,cat} < K_{d,str}$, it is possible that $K_{d,str}(k_1/k_2) \ll [Mg^{2+}] \ll K_{d,cat}(k_2/k_3)$. When these conditions are met, channel 2 is the major contributor to k_{obs} and the slope of a log k_{obs}−log$[Mg^{2+}]$ plot will approach unity as per eq 13b.

In addition to considerations of the Mg^{2+} concentration dependence of the reaction, multiplateau behavior may be observed. Under conditions in which $K_{d,str} \ll [Mg^{2+}] \ll K_{d,cat}$, binding of the structural metal ion should level off if $K_{d,str}(k_1/k_2) \ll [Mg^{2+}] \ll K_{d,cat}(k_2/k_3)$. Simulations were carried out using Excel to study the shape of the curves and the value of the Hill constant under various limiting solution conditions (see Results).

Consideration of Error in the Brønsted Analysis. The Brønsted coefficient, β, for general base catalysis was calculated from the Brønsted equation [log $k_B = \beta(pK_a)$ + log G_B] using rate constants for water and hydroxide ion, and pK_a values for their conjugate acids (*17*). The term k_B is the observed rate constant in a certain base, and G_B is a constant specific to the reaction being studied. The slope of the line, β, was calculated as $[\log(k_{OH^-}/k_{solv})]/\Delta pK_a$, which is $\{\log[(2.8 \times 10^3\ M^{-1}\ min^{-1})/(0.0034\ min^{-1}/55\ M)]\}/(15.7 - -1.7) = 0.44$. The error in k_{OH^-} was estimated to be $(2.8 \pm 2.2) \times 10^3\ M^{-1}\ min^{-1}$, and the error in k_{solv} to be $(6.2 \pm 2.5) \times 10^{-5}\ M^{-1}\ min^{-1}$ (see the legend of Figure 3). A conservative estimate of error can be obtained from the following simple analysis. If the maximum in k_{OH^-} and the minimum in k_{solv} are considered, β can be calculated as 0.47. Likewise, the minimum in k_{OH^-} and the maximum in k_{solv} gave a β value of 0.39. Thus, the error in β is estimated to be 0.44 ± 0.05. Despite uncertainty in the values of k_{solv} and k_{OH^-}, β is a fairly robust parameter because the logarithm of k is taken, and the values that are used are separated by a large difference in pK_a.

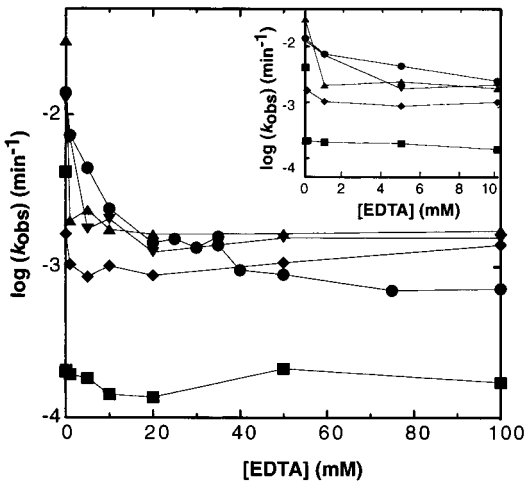

FIGURE 2: Effect of Na_2EDTA concentration on k_{obs}. Experiments were carried out at pH 5.0 (●), 5.5 (▼), 6.0 (▲), 7.0 (◆), and 8.0 (■) with Chelex 100-treated reagents and 1 M NaCl and in the absence of added divalent metal ion. The inset shows the 0−10 mM Na_2EDTA data in detail.

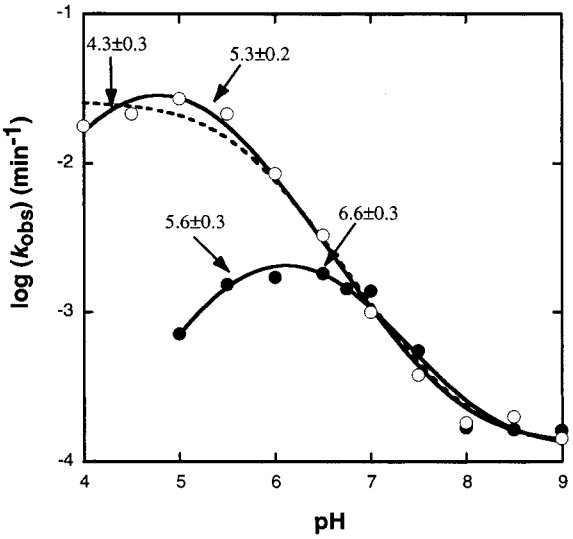

FIGURE 3: Effect of pH on k_{obs} in the absence of added divalent metal ions. Reactivity−pH profiles observed in a 1 M NaCl, 1 mM EDTA solution (○) (*2*) and in a 1 M NaCl, 100 mM EDTA solution treated with Chelex 100 (●) are shown. Data for a 1 M NaCl, 1 mM EDTA solution were fit to eq 7 (- - -; $R^2 = 0.988$) to give the following values: $pK_{a2} = 5.6 \pm 0.1$, $k_{solv} = 0.026 \pm 0.004$ min^{-1}, and $k_{OH^-} = (3.1 \pm 1.2) \times 10^4$ M^{-1} min^{-1}. Data for a 1 M NaCl, 1 mM EDTA solution were also fit to eq 8 (—; $R^2 = 0.995$) to give the following values: $pK_{a1} = 4.3 \pm 0.3$, $pK_{a2} = 5.3 \pm 0.2$, $k_{solv} = 0.048 \pm 0.017$ min^{-1}, and $k_{OH^-} = (6.5 \pm 3.0) \times 10^4$ M^{-1} min^{-1}. Data for a 1 M NaCl, 100 mM EDTA solution were fit to eq 8 (—; $R^2 = 0.958$) to give the following values: $pK_{a1} = 5.6 \pm 0.3$, $pK_{a2} = 6.6 \pm 0.3$, $k_{solv} = 0.0034 \pm 0.0014$ min^{-1}, and $k_{OH^-} = (2.8 \pm 2.2) \times 10^3$ M^{-1} min^{-1}. Data for a 1 M NaCl, 100 mM EDTA solution could not be well fit to eq 7. Observed pK_a values for fits to eq 8 are provided in the figure.

Structural Models and Programs. Electrostatic potential calculations were carried out using numerical solutions to the nonlinear Poisson−Boltzmann (NLPB) equation. Calculations were carried out using a modified form of DelPhi that utilizes a finite difference multigridding algorithm (*18*, *19*). This approach was recently used in reports of NLPB calculations on RNA (*20*−*22*). Structural coordinates were obtained from the Protein Data Bank (PDB) for the hepatitis delta virus ribozyme (PDB entry 1cx0) (*5*), fragment I of 5S rRNA (PDB entry 364d) (*23*), and the P4−P6 domain of the *Tetrahymena* group I intron (PDB entry 1gid) (*24*). Hydrogen atoms were added using REDUCE (*25*), and bound metal ions and water molecules were omitted from the NLPB calculations.

In general, calculations were performed in a fashion similar to that published previously (*20*). Each atom was placed in a medium with a low dielectric constant ($\epsilon_m = 2$) defined by the solvent accessible surface-enclosed volume, which was obtained using a probe radius of 1.4 Å. The solvent was treated as a continuum with a dielectric of 80, containing a 1:1 electrolyte. A 2.0 Å ion exclusion radius (Stern layer) was added to the surface of the RNA to approximate a hydrated sodium ion. A salt concentration of 0.15 M was used in the calculations, except for the P4−P6 domain, which had to be calculated with a salt concentration of 0.25 M for the solution to converge (*20*). Atomic radii and partial charges were defined using the cvff91 parameter set from DISCOVER (MSI). Calculations were performed using a 65 × 65 × 65 cubic lattice, and potentials were calculated using a two-step focusing procedure (*26*). Initial potentials were approximated analytically at lattice points on the boundary of the grid using the Debye−Hückel equation (*27*), and solutions were obtained for 0, 0.05, 0.10, and 0.15 M salt using boundary conditions interpolated from the previous step. Potentials were iterated to a convergence of $< 1 \times 10^{-4} kT/e$. Three-dimensional structures and electrostatic potentials were rendered using GRASP (*28*). Figures are displayed using scaled potentials ranging linearly from $-40kT/e$ to $40kT/e$ to accommodate the large negative charge of the ribozyme.

RESULTS

Effect of High Concentrations of Na_2EDTA on the Reaction Rate. The genomic and antigenomic HDV ribozymes self-cleave in a variety of divalent metal ions. The ribozyme has equal or somewhat greater activity in Ca^{2+} than in Mg^{2+}, and is also active to varying degrees in Ba^{2+}, Sr^{2+}, Mn^{2+}, Co^{2+}, and other divalent metal ions (*2*, *7*, *29*). The metal ion promiscuity of the ribozyme indicates that caution should be exercised in removing trace amounts of polyvalent metal ions from the solution.

The genomic HDV ribozyme can also self-cleave in the absence of added divalent metal ions, and the pH dependence of the reaction under these conditions is of mechanistic interest (*2*). Previously, we compared the reaction rate in 1 and 2 mM Na_2EDTA at pH 7.0 in the absence of added divalent metal ions. However, further analysis has revealed that 1 mM Na_2EDTA is insufficient to complex all of the contaminating divalent metal ions in the solution at lower pH values (Figure 2). This appears to be due to EDTA binding polyvalent metal ions less tightly at lower pH due to protonation of its acetate functional groups (*13*).

We examined the effect of large concentrations of Na_2-EDTA on k_{obs} under several pH conditions (Figure 2). At a high pH value of 7.0 or 8.0, k_{obs} is independent of Na_2EDTA concentration from 1 to 100 mM, consistent with the previous study (*2*). However, at pH <6.0, k_{obs} decreases upon addition of >1 mM Na_2EDTA. For example, at pH 5.0, ≈75 mM Na_2EDTA was required before the rate was level with respect to EDTA addition (Figure 2). The inhibitory effect of Na_2-

EDTA does not appear to be due to changes in the ionic strength of the solution. These experiments were conducted in the presence of 1 M NaCl, so the order of magnitude increase in Na^+ concentration upon Na_2EDTA addition was modest (Figure 2). Also, addition of Na_2EDTA from 1 to 100 mM did not lead to inhibition at pH 7.0 or 8.0, under which conditions contaminating divalent metal ions were presumably already scavenged (Figure 2). Under similar conditions of no added Mg^{2+}, citric acid added to 100 mM did not inhibit the reaction at pH 6.0 and 1 mM EDTA (data not shown). Citric acid mimics the functionality of EDTA and should have all three of its carboxylates nearly completely deprotonated at pH 6.0 (*14*, *30*). However, citric acid binds Mg^{2+} $\approx 10^5$ times weaker than EDTA (*14*, *30*), suggesting that EDTA leads to slower reaction by scavenging divalent metal ions. Experiments conducted in 1 M NaCl, 1 M KCl, or 1 M NH_4Cl, all in the presence of 10 mM $MgCl_2$, gave similar values of k_{obs} between 4.0 and 4.6 min^{-1}, suggesting that the identity of the monovalent cation is not important (data not shown). Thus, the effect of EDTA concentration on reducing k_{obs} at low pH appears to reflect weaker binding of contaminating divalent metal ions to EDTA.

Treating the solutions with Chelex resin lowered the contaminating metal ion concentration from $\approx$10 to 2 μM divalent ions (as Mg^{2+}) but did not completely remove all ions. This analysis was based upon dissociation constants determined for EDTA and Mg^{2+} and the pK_a values for EDTA, as well as fitting of the data at low EDTA concentrations (see below). Our inability to lower the contaminating divalent metal ion concentration further likely reflects the poor affinity of Chelex resin for alkaline earth metal ions versus transition metal ions (*12*). Moreover, on the basis of the properties of structurally related EDTA, Chelex should have a weaker affinity for divalent metal ions at high ionic strengths, making preparation of metal-free stock salt solutions problematic. It appears that under the solution conditions of no added divalent metal ion, high NaCl concentration, and low pH, which are of interest to ribozyme mechanism studies, it is not possible to remove all divalent metal ions from the solution with confidence. Under such conditions, use of a metal-buffered system (*15*) appears to be necessary to reduce the concentration of free metal ions to an acceptable level.

pH Dependence of the Reaction in 100 mM Na_2EDTA. We examined the pH dependence of the reaction kinetics in the absence of added divalent ions and the presence of 100 mM Na_2EDTA (Figure 3). According to Figure 2, 100 mM Na_2EDTA is sufficient to provide EDTA-independent kinetics at pH 5−8. The pH dependence of the reaction in the presence of 1 mM Na_2EDTA (*2*) is compared to that in 100 mM Na_2EDTA (Figure 3). The overall shapes of the curves are similar, with identical values of k_{obs} obtained at high pH. However, at lower pH, the rate is 10−40-fold slower in the presence of 100 mM Na_2EDTA. This difference likely reflects the inability of 1 mM EDTA to sequester all divalent ions at low pH. These data also suggested that low concentrations of divalent metal ions may stimulate self-cleavage under low-pH conditions. Similar effects of EDTA and Mg^{2+} binding at low pH were recently reported (*31*).

The shape of the pH−reactivity curve in the absence of free divalent ions is of particular interest. The fits of the data were to eq 7 or 8, derived from the kinetic model in Scheme 1. This model incorporates four ionization states of the ribozyme, with the active species being one of the two hemiprotonated states. It appears that the residues involved in protonation are C75 and C41. Protonation of C75 is depicted in the functional species based upon a published model in which C75 serves as the general acid and $[Mg(OH)]^+$ as the general base under physiological salt conditions of $\approx$1 mM Mg^{2+} (*2*). [This issue is discussed below, but it should be noted that kinetically equivalent models in which C75 serves as the general base in the reaction can also explain the data (*1*, *32*).] At low pH, the ribozyme is shown in an inactive, doubly protonated form, and the other residue protonated may be C41, although its identity is not critical to the conclusions drawn herein (see Discussion). The doubly protonated form of the ribozyme explains the inhibition at pH <6 (100 mM EDTA; Figure 3). A fit to eq 7, which does not account for this low-pH feature, is also shown for the 1 mM EDTA case. In all cases, superior fits were obtained for eq 8.

Another feature of the model in Scheme 1 is that the active ribozyme species can react by two Mg^{2+}-independent channels, channel 1′ and channel 1″. Channel 1′ is shown with a first-order rate constant k_{solv}, and channel 1″ with an apparent first-order rate constant $k_{OH^-}[OH^-]$. The rate constant for channel 1′ requires a general base that is present at a pH-independent concentration, and Brønsted analysis is consistent with this being solvent water (see Discussion). Participation of hydroxide ion in channel 1″ accounts for the pH independence of the high-pH portion of the reaction, since the increase in the hydroxide ion concentration can offset the decrease in the $C75H^+$ concentration.

Self-Cleavage over a Wide Range of Mg^{2+} Concentrations. Addition of EDTA to solutions that were treated with Chelex resin still resulted in further inhibition of cleavage, especially at low pH (Figure 2). This observation suggested that very low concentrations of divalent metal ions accelerate the reaction. We therefore examined the Mg^{2+} dependence of the reaction from nanomolar to near-molar concentrations of Mg^{2+}.

The folding of large RNAs such as the HDV ribozyme is dependent on the presence of cations. In an attempt to decouple the effect of divalent metal ions on catalysis from their effects on folding, titrations were conducted in the presence of high concentrations of NaCl, which has been shown to induce tertiary folding of large RNAs (*33*). To control the concentration of free Mg^{2+} in the presence of NaCl and contaminating divalent metal ions, we first determined the affinity of EDTA for Mg^{2+} at various ionic strengths, and then used an EDTA/metal ion buffering system. As expected, Mg^{2+} binds tighter to EDTA at high pH and low ionic strength (Figure 4A). We also wanted to know EDTA−Mg^{2+} affinities at pH >7, but it was not possible to directly determine $K_{d,EDTA-Mg}$ due to very strong binding and uncertainty at low Mg^{2+} concentrations. As an alternative, we took advantage of the log−linear relationship between $K_{d,EDTA-Mg}$ and α^{4-} (see Methods). To calculate α^{4-} (eq 2), we determined the pK_a values for the third and fourth ionization equilibria of EDTA by titration and fitting to eq 3 (Figure 4B). The pK_a values determined at high ionic strengths at 37 °C were shifted to the acidic side relative to 0.1 M ionic strength values in the literature (*14*). The plot

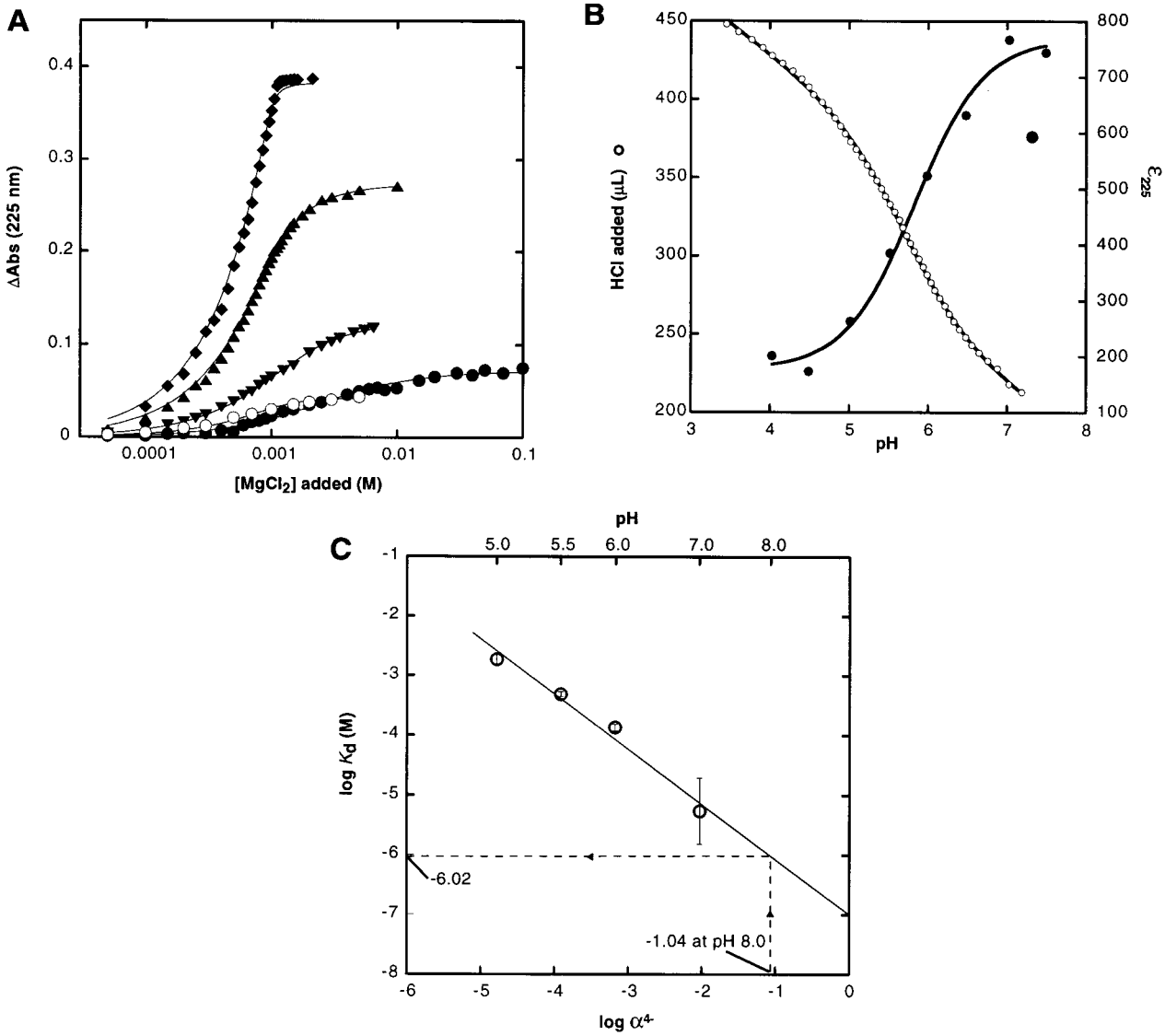

FIGURE 4: Effect of pH and ionic strength on Mg^{2+} binding to Na_2EDTA at 37 °C. (A) Absorbance change at 225 nm upon addition of $MgCl_2$ to 1 mM EDTA at pH 5.0 (●), 5.5 (▼), 6.0 (▲), and 7.0 (◆) in a 1 M NaCl solution, and at pH 5.0 (○) without NaCl; the lines are fits to eq 1 and give $K_{d,EDTA-Mg}$ values of 1.9 ± 0.1, 0.49 ± 0.02, 0.13 ± 0.01, 0.0055 ± 0.0029, and 0.12 ± 0.04 mM, respectively. (B) Determination of $pK_{a3,EDTA}$ in 1 M NaCl at 37 °C. Lines are fits to eq 3. The HCl titration using a glass electrode gave a pK_{a3} of 5.74 ± 0.04. Values for these data correspond to the left-hand *y*-axis. Similar experiments carried out between pH 7.5 and 10.75 gave a pK_{a4} of 9.02 ± 0.03 (data not shown). Values for pK_{a3} and pK_{a4} at room temperature with 0.1 M NaCl were also determined and were in good agreement with the literature (ref *14* and data not shown). The pH dependence of the absorbance change at 225 nm was converted to a change in extinction coefficient and fit to eq 3 in which the slopes of the baselines were set to zero; this was done to reduce the number of parameters because the slopes were too close to zero to determine accurately. This resulted in a pK_{a3} of 5.83 ± 0.08 (similar to that obtained by the pH meter titration). Values for these data correspond to the right-hand *y*-axis. In all cases, values and errors for the slopes and intercepts of the upper and lower baselines were reasonable. (C) Dependence of log $K_{d,EDTA-Mg}$ on log α^{4-}. The value of α^{4-} was calculated at each pH using eq 2 and the values of pK_{a3} and pK_{a4} determined in panel B using the glass electrode method. The linear fit had a slope of −0.92 ± 0.10, within experimental error of the theoretical value of −1, and an intercept of −7.0 ± 0.4. The intercept gives a $K_{d,MY}$ of 100 nM at 1 M NaCl, which is somewhat larger than the value of 2 nM at 0.1 M NaCl (25 °C) (*14*), as expected. Using the linear relationship of log $K_{d,EDTA-Mg}$ and log α^{4-} allowed $K_{d,EDTA-Mg}$ to be estimated at pH >7.0. An example for pH 8.0 is given in the figure, and indicated with a dashed line.

of log $K_{d,EDTA-Mg}$ versus log α^{4-} was linear with a slope near −1, and the value of $K_{d,MY}$ was −7.0, somewhat weaker than at an ionic strength of 0.1 M (*14*) (Figure 4C). Values for $K_{d,EDTA-Mg}$ at higher pH values were then determined by extrapolation.

The effect of varying the concentration of uncomplexed Mg^{2+} on log k_{obs} in the presence of 1 M NaCl is shown in Figure 5. At low concentrations of Mg^{2+}, between $<10^{-9}$ and 10^{-7} M, the rate was independent of Mg^{2+} concentration. This result is consistent with a Mg^{2+}-free component to folding and cleavage, represented by channel 1 (Scheme 2). The dependence of log k_{obs} on pH under these conditions is provided in the inset of Figure 5 and in Figure 3. Addition of intermediate concentrations of Mg^{2+} from $\approx 10^{-7}$ to 10^{-4} M led to a log−linear dependence of k_{obs} on Mg^{2+} concentration. This observation indicates that Mg^{2+} is facilitating self-cleavage in some manner. The dependence of log k_{obs} on pH under these conditions is qualitatively similar to that seen in the absence of Mg^{2+} stimulation (Figure 5 inset). This observation suggests that even though Mg^{2+} is stimulating the reaction it is not acting as the general base. Apparently, Mg^{2+} ions have roles in the reaction other than

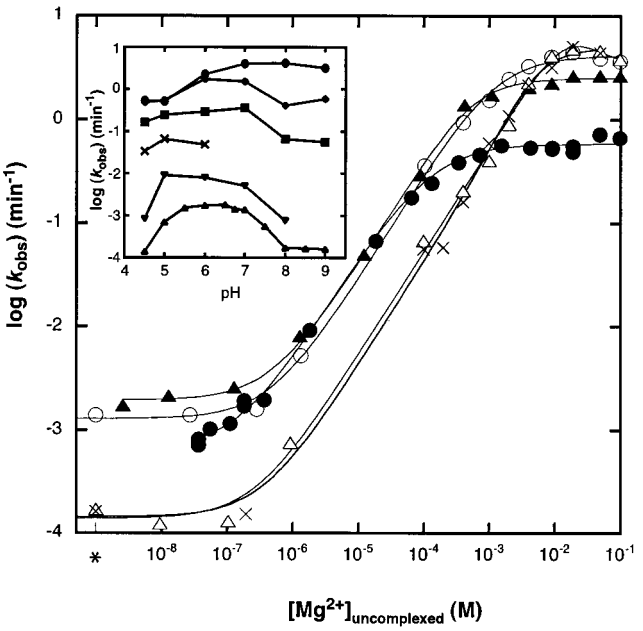

FIGURE 5: Effect of Mg^{2+} on k_{obs} in the presence of 1 M NaCl at 37 °C. Reactivity−$[Mg^{2+}]_{uncomplexed}$ profiles at representative pH values are shown: pH 5.0 (●), 6.0 (▲), 7.0 (○), 8.0 (△) and 9.0 (×). The $K_{d,EDTA-Mg}$ values determined in Figure 4 were used to determine $[Mg^{2+}]_{uncomplexed}$ values according to eq 4. Reactions were carried out with a mixture of EDTA and Mg^{2+}, as described in Methods. The data with the asterisk (*) is k_{obs} in the presence of 100 mM EDTA without added $MgCl_2$. Estimates of free $MgCl_2$ concentration are 1.1×10^{-10}, 1.9×10^{-11}, and 3.9×10^{-11} M at pH 7.0, 8.0, and 9.0, respectively, based on values of $K_{d,EDTA-Mg}$ and estimates of the contaminating metal ion concentration as ≈2 μM Mg^{2+}. Fits are to eqs 9a−9d; the only parameters that could be reliably determined from these experiments were k_1 and another rate constant, which could be k_2, k_3, or a combination of the two depending on the pH. Values of k_1 can also be obtained from Figure 3, and k_{max} is provided in Table 1. Nevertheless, the plateau regions and the slopes of the curves are interpretable as described in the text. The inset shows reactivity−pH profiles in the presence of 100 mM EDTA without added $MgCl_2$ (▲) and at approximately 1 μM (▼), 10 μM (×), 100 μM (■), 1 mM (◆), and 10 mM (●) uncomplexed Mg^{2+}.

catalysis, presumably to fold the ribozyme (see below). This feature of the reaction is depicted in channel 2 of Scheme 2, in which the ribozyme reacts with a new rate constant, k_2, but does so without the catalytic metal ion.

Addition of higher concentrations of Mg^{2+}, from 10^{-4} to 10^{-1} M, led to saturation behavior (Figure 5). The dependence of log k_{obs} on pH under these conditions is inverted from that observed at low and intermediate Mg^{2+} concentrations (Figure 5 inset). This change in the pH profile is indicative of direct participation of hydroxide ion from $[Mg(OH)]^+$ or solvent in the reaction as a general base (see Discussion). This feature of the reaction is depicted in channel 3 of Scheme 2 in which the ribozyme reacts with a third rate constant, k_3. These data, combined with those at lower Mg^{2+} concentrations, suggest that Mg^{2+} ions can play diverse roles in the ribozyme mechanism depending on solution conditions, serving both to fold the ribozyme and to catalyze bond cleavage.

Developing the Multichannel Model with Further Experiments. The dependence of k_{obs} on Mg^{2+} concentration was further examined over the micromolar to near-molar concentration range at a series of pH values (Figure 6). The plots in Figure 6 are semilogarithmic to facilitate examination of local features of the plots, and no-added NaCl data are shown for comparison. Fits to the 1 M NaCl data were either to the Hill equation (eq 10) or to eqs 9a−9d derived from the multichannel model. The Hill equation was used because in many cases fitting of individual data sets to eqs 9a−9d resulted in one or more of the parameters having large error; nevertheless, the robust parameters from fits to eqs 9a−9d were similar to those from fits to eq 10.

The observed Mg^{2+} dissociation constants at 0 and 1 M NaCl have opposing pH trends. At pH 5.0 without NaCl, an observed K_d of 14 mM was obtained (Figure 6A and Table 1). In contrast, fitting of the 1 M NaCl data to the Hill equation resulted in a K_d of 0.19 mM and a Hill constant of 0.82 (Table 1). These data are consistent with binding of one Mg^{2+} ion at 1 M NaCl, which binds tighter than that observed without NaCl. As the pH is increased, binding of the Mg^{2+} without NaCl is strengthened, while binding at 1 M NaCl is weakened (Figure 6 and Table 1). These opposing pH trends are consistent with a model involving two or more different Mg^{2+} ions. The divalent metal ion observed without NaCl appears to be a catalytic outer-sphere metal ion which has negative linkage with protonation of C75 (*2*). On the basis of opposing behavior, the second Mg^{2+} ion observed in 1 M NaCl is proposed to serve a structural role. Apparently, Mg^{2+} ions can further stabilize a native ribozyme fold only partially induced by 1 M NaCl (see Discussion).

The data in Figure 6 show several deviations from behavior expected for binding of a single ion. At pH 5.0 and high Mg^{2+} concentration, a second increase in rate occurs. This behavior can be modeled by assuming this reflects binding of another functional Mg^{2+} ion which has a K_d of ≈160 mM. This value is only 10-fold weaker than the K_d observed without NaCl for the catalytic metal ion (Table 1), and is subject to substantial error (Figure 6). Therefore, this weaker binding ion may represent the catalytic metal ion, with modest salt dependence for its K_d. Consistent with this interpretation, there appears to be little involvement of the catalytic metal ion at pH 5.0 and 10 mM Mg^{2+}, based upon the leveling off of k_{obs} between pH 5.0 and 4.0 (Figure 5 inset).

At pH 6.0 and 1 M NaCl, the data were reasonably well described with a Hill equation and a Hill constant of 0.84 (Figure 6B and Table 1). To test for the presence of a second divalent metal ion, the experiment was repeated at 0.1 M NaCl, which might strengthen binding of the divalent metal ions differentially. Under these conditions, there appears to be a leveling off of k_{obs} centered at ≈1 mM Mg^{2+} followed by an increase in k_{obs} with further Mg^{2+} addition, showing a K_d of ≈30 mM with a modest salt dependence. This behavior could be modeled better with eqs 9a−9d for the multichannel model than with the Hill equation (Figure 6B inset).

Due to the opposing pH trends of the K_d values for the divalent metal ions, we expected the catalytic metal ion to bind tighter than the structural ion at high pH, possibly resulting in cooperative behavior for an ordered mechanism (Scheme 2). Plots of k_{obs} versus Mg^{2+} at pH 8.0 and 9.0 were best described by α_H values of 1.8 and 1.5, respectively (Figure 6D and Table 1), and no indication of leveling off was observed at intermediate Mg^{2+} concentrations. This effect suggests that binding of the catalytic metal ion is dependent on binding of the structural ion, possibly because the structural ion facilitates creation of the catalytic metal

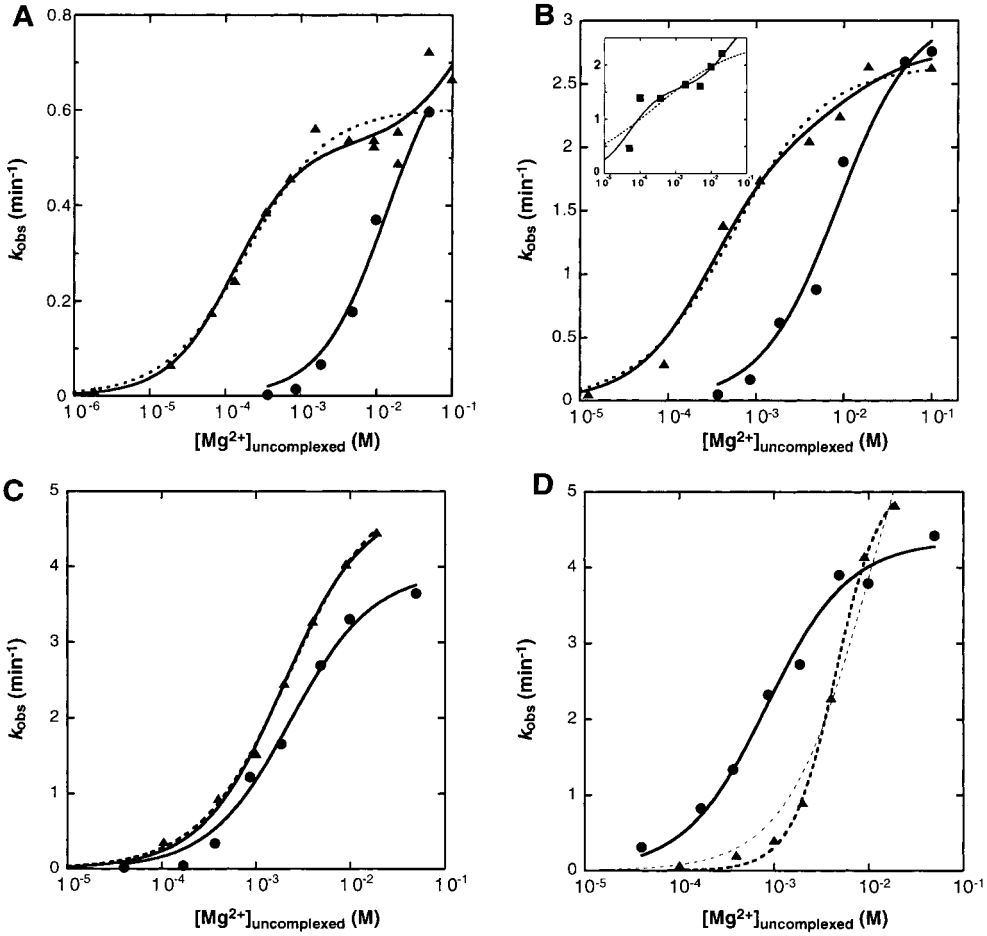

FIGURE 6: Comparison of reactivity−[Mg^{2+}]$_{uncomplexed}$ profiles at various pH values in the presence of 0.1 (■) and 1 M NaCl (▲), and in the absence of added NaCl (●). Panels A−D are for pH 5.0, 6.0, 7.0, and 8.0, respectively. Data for 0.1 and 1 M NaCl were fit to the Hill equation (eq 10) (thick dashed line), or to a modified multichannel model equation (eqs 9a−9d) (solid line) in which the k_1f_1 term was set to zero since very low Mg^{2+} concentration data were not used in these fits. In general, the two fits yielded similar values of k_2 (eqs 9a−9d) and k_{max} (eq 10), and of one K_d term (eqs 9a−9d) and K_d from the Hill equation (eq 10); the exception was pH 8.0 data for which reliable kinetic and thermodynamic constants could not be obtained for eqs 9a−9d due to the apparent cooperativity of Mg^{2+} binding. For the pH 8.0, 1 M NaCl data, a fit to eq 10 in which α_H was fixed at 1 (thin dashed line; $R^2 = 0.979$) is shown for comparison to the Hill fit (thick dashed line; $R^2 = 0.998$). The parameters from nonlinear least-squares fits to the Hill equation (eq 10) are provided in Table 1, and parameters from selected fits to eqs 9a−9d are given here. The pH 5.0 data at 1 M NaCl and pH 6.0 data at 0.1 M NaCl revealed apparent upward curvature at the highest Mg^{2+} concentrations that were tested, which was fit by eqs 9a−9d to the multichannel model. Fitting of the data at pH 5.0 and 1 M NaCl resulted in the followinh values: $k_2 = 0.53 \pm 0.03$ min^{-1}, $k_3 = 0.96 \pm 0.7$ min^{-1}, $K_{d,str} = 0.13 \pm 0.03$ mM, and $K_{d,cat} = 160 \pm 400$ mM. R^2 values for the pH 5.0, 1 M NaCl data were as follows: 0.992 for the multichannel model (solid line) and 0.986 for the Hill fit (thick dashed line). At pH 6.0 and 0.1 M NaCl, the constant k_3 was forced to be 3.0 based on the k_{max} values of 2.6 and 2.9 in 1 M NaCl and without NaCl at pH 6.0, respectively; fits to the modified multichannel model of eqs 9a−9d resulted in the following values: $k_2 = 1.6 \pm 0.3$, $K_{d,str} = 0.05 \pm 0.03$ mM, and $K_{d,cat} = 0.03 \pm 0.02$ mM. R^2 values for the pH 6.0, 0.1 M NaCl data were as follows: 0.930 for the multichannel model (solid line) and 0.865 for the Hill fit (thick dashed line). All no-added NaCl data were fit to a binding isotherm for a single ion (solid line) (*2*), which is eq 10 in which α_H was fixed to 1. Kinetic and thermodynamic constants for no-added NaCl data are reported in Table 1 (*2*).

Table 1: Constants for Mg^{2+} Binding to the Ribozyme at 1 M NaCl from the Hill Equation[a]

pH	α_H	K_d (mM)	k_{max} (min^{-1})
4.5	1.4 ± 0.2	0.14 ± 0.01 (16 ± 3)[b]	0.52 ± 0.01 (0.25 ± 0.02)[b]
5.0	0.82 ± 0.16	0.19 ± 0.05 (14 ± 3)[b]	0.60 ± 0.03 (0.78 ± 0.06)[b]
6.0	0.84 ± 0.12	0.54 ± 0.10 (9.7 ± 2.0)[b]	2.6 ± 0.1 (3.2 ± 0.3)[b]
7.0	0.92 ± 0.06	2.2 ± 0.2 (2.4 ± 0.4)[b]	5.1 ± 0.2 (3.9 ± 0.2)[b]
8.0	1.85 ± 0.14	4.5 ± 0.3 (0.86 ± 0.1)[b]	5.2 ± 0.2 (4.3 ± 0.1)[b]
9.0	1.5 ± 0.3	4.8 ± 0.96 (ND)[c]	5.0 ± 0.4 (ND)[c]

[a] The Hill equation is eq 10. [b] Kinetic and thermodynamic parameters at no-added NaCl are given in parentheses (*2*). All no-added NaCl data were fit to a binding isotherm for a single ion, which is eq 10 in which α_H was fixed to 1. [c] Not determined.

site. The effect of NaCl concentration on the affinity of the catalytic metal ion appears to be modest when compared to values measured without NaCl (Table 1). For example, at pH 8.0, the observed K_d is only 5-fold weaker than K_d for binding of the catalytic metal ion without NaCl, and the observed K_d is likely an upper limit for the K_d for the catalytic ion in 1 M NaCl at pH 8.0. Values of α_H measured between pH 5.0 and 7.0 are between 0.82 and 0.92 (Table 1). The value of α_H measured at pH 4.5 is 1.4, which is larger than expected (Table 1). This may due to the inhibition of cleavage at very low pH being severe (Figure 5), possibly resulting in cooperative binding of several structural metal ions (see the evidence for multiple structural metal ions below).

Comparing Results to Simulations of the Multichannel Model. Simulations of the data in Figures 5 and 6 were carried out using rate and binding constants similar to those

determined from experiments. This simulation was used to define the expectations of the kinetics under various conditions, to test fitted values of α_H, and to make predictions on the metal ion dependence of the reaction. At low pH and very low Mg^{2+} concentrations, the log k_{obs} versus log[Mg^{2+}] profile is predicted to have a Mg^{2+}-independent portion, which is dominated by reaction down channel 1 (eq 13a; compare Figure 5 and panels A and B of Figure 7). At low pH and intermediate Mg^{2+} concentrations, the log k_{obs} versus log[Mg^{2+}] profile is predicted to have a slope of 1, which is dominated by reaction down channel 2 (eq 13b; compare Figure 5 and panels A, B, and D of Figure 7). When these data are plotted on a semilogarithmic scale, the simulation shows an intermediate leveling off of k_{obs} near 1 mM Mg^{2+} followed by an increase at higher Mg^{2+} concentrations (Figure 7C; see Methods for conditions). Fitting of the simulated 1 mM and lower-Mg^{2+} concentration data to the Hill equation gives an α_H of 0.96 and a K_d similar to that input into the simulation (Figure 7C). These features are consistent with the experimental data (Figure 6A, Figure 6B inset, and Table 1).

Simulations using pH 8.0 data and low Mg^{2+} concentrations show that the log k_{obs} versus log[Mg^{2+}] profile is predicted to have a Mg^{2+} concentration-independent portion, which is dominated by reaction down channel 1 (eq 13a; compare Figure 5 and panels E and F of Figure 7). At high pH and intermediate Mg^{2+} concentrations, there is a contribution of channel 2 to the reaction (Figure 7E,F,H). This may seem surprising given that binding of the two divalent metal ions is cooperative (Figure 6D, Table 1, and Figure 7G). However, this feature can be rationalized if the rate constant for channel 2 is considerably larger than that for channel 1. This leads to a substantial fraction of the total reaction going down channel 2 even though the occupancy of the channel 2 ribozyme−Mg^{2+} species is relatively small (Figure 7F). A slope of 1 is therefore expected at intermediate Mg^{2+} concentrations, consistent with experiments (compare Figure 5 and panels E and H of Figure 7). At high pH and high Mg^{2+} concentrations, the rate is dominated by channel 3. Simulations predict that the slope of k_{obs} versus log[Mg^{2+}] profile should show no intermediate leveling off and fits to eq 10 should give an α_H of ≈1.7, consistent with experiments (eq 13c; compare Figure 6D, Table 1, and panels G and H of Figure 7).

Evidence for Multiple Structural Divalent Metal Ions. Mg^{2+} titrations of the self-cleaved form of the ribozyme were carried out at pH 7.0 with absorbance detection at 260 and 280 nm in the presence of 1 M NaCl (Figure 8). From UV melting experiments at 260 nm, there is not a transition near 37 °C in the presence of 1 M NaCl or >0.1 mM $MgCl_2$ (data not shown). Data were fit to a binding model involving cooperative binding of multiple divalent metal ions, using a modified version of the Hill equation that allows for sloping baselines (eq 5). Fits to both the 260 and 280 nm data were optimal with an α_H of ≈5, while poor fits were obtained with an α_H of 1 (Figure 8). If the catalytic metal ion binds considerably weaker to the self-cleaved form the ribozyme, then the catalytic metal may not be observed in the absorbance titrations on the self-cleaved form (see Discussion). The observed K_d from the absorbance titrations was ≈0.4 mM (Figure 8), while those obtained from the functional assay were ≈2 mM (Table 1). The 5-fold difference in K_d values between the two methods may be because the Hill K_d values are semiempirical and reflect averaging of the other metal ions, or because the Mg^{2+} binding to the cleaved ribozyme is tighter than that to the ribozyme having the catalytic Mg^{2+} ion. The increase in absorbance in the transition region may indicate that preformed alternate secondary structure has to rearrange prior to tertiary structure formation.

To test for divalent metal ion binding site candidates, we carried out a series of electrostatic potential calculations on the ribozyme using solutions to the NLPB equation. In general, these calculations have been shown to give reasonable descriptions of the electrostatic properties of nucleic acids based on comparison to a number of biophysical properties, including pK_a shifts, EPR measurements, salt effects on ligand binding, and metal ion binding (*20*, *21*). To begin, we performed calculations on two RNAs that have published surface potentials (*20*), fragment I of 5S rRNA (*23*) and the P4−P6 domain of *Tetrahymena* (*24*). Our calculated surface potentials were similar to those published (data not shown and ref *20*). Inspection revealed a nearly identical correspondence of regions of negative and positive potential, and representative sampling of the magnitude of the potential gave values similar to those published.

In Figure 9, the calculated surface potential for the self-cleaved form of the HDV ribozyme is shown from three views rotated by 120°. The refined model of the self-cleaved form of the ribozyme contains nine site-bound magnesium ions near the ribozyme portion of the structure (*5*); these are shown in Figure 9, although they were not included in the calculation. We found that seven of these ions are located within 5 Å of regions of negative potential of less than $-30kT/e$. The cutoff of $-30kT/e$ was chosen on the basis of the observation that isolated A-form helices in the ribozyme, such as P2, had potentials ranging from 0 to $-25kT/e$, similar to previously reported potentials for A-form RNA (*20*). Preferential localization of metal ions to regions of exceptional negative potential is expected on the basis of results for other RNAs (*20*, *22*, *34*). In addition, an extensive cleft with high negative potential was found near the active site, although well-resolved metal ions were not found here (*5*) (see Discussion). Overall, the electrostatic calculations revealed numerous regions of negative potential, many of which have crystallographically resolved metal ions nearby, and other regions that may attract metal ions not resolved in the crystal structure.

DISCUSSION

The hairpin, hammerhead, and VS ribozymes have been shown to undergo self-cleavage at high concentrations of Na_2EDTA (*9*), and this has called into question the catalytic role of divalent metal ions in the chemical step of these ribozymes (*9*, *35*, *36*). The recently determined crystal structure of the hairpin ribozyme does not have metal ions at the active site, but instead reveals RNA bases that may serve as general acid−base catalysts (*37*). In addition, crystallographic results for the self-cleaved form of the HDV ribozyme provide no evidence for well-ordered metal ions at the expected site of catalysis (*4*). We previously reported that the genomic HDV ribozyme is active in 1 M NaCl, in 1−2 mM EDTA at pH 7.0, and in the absence of added

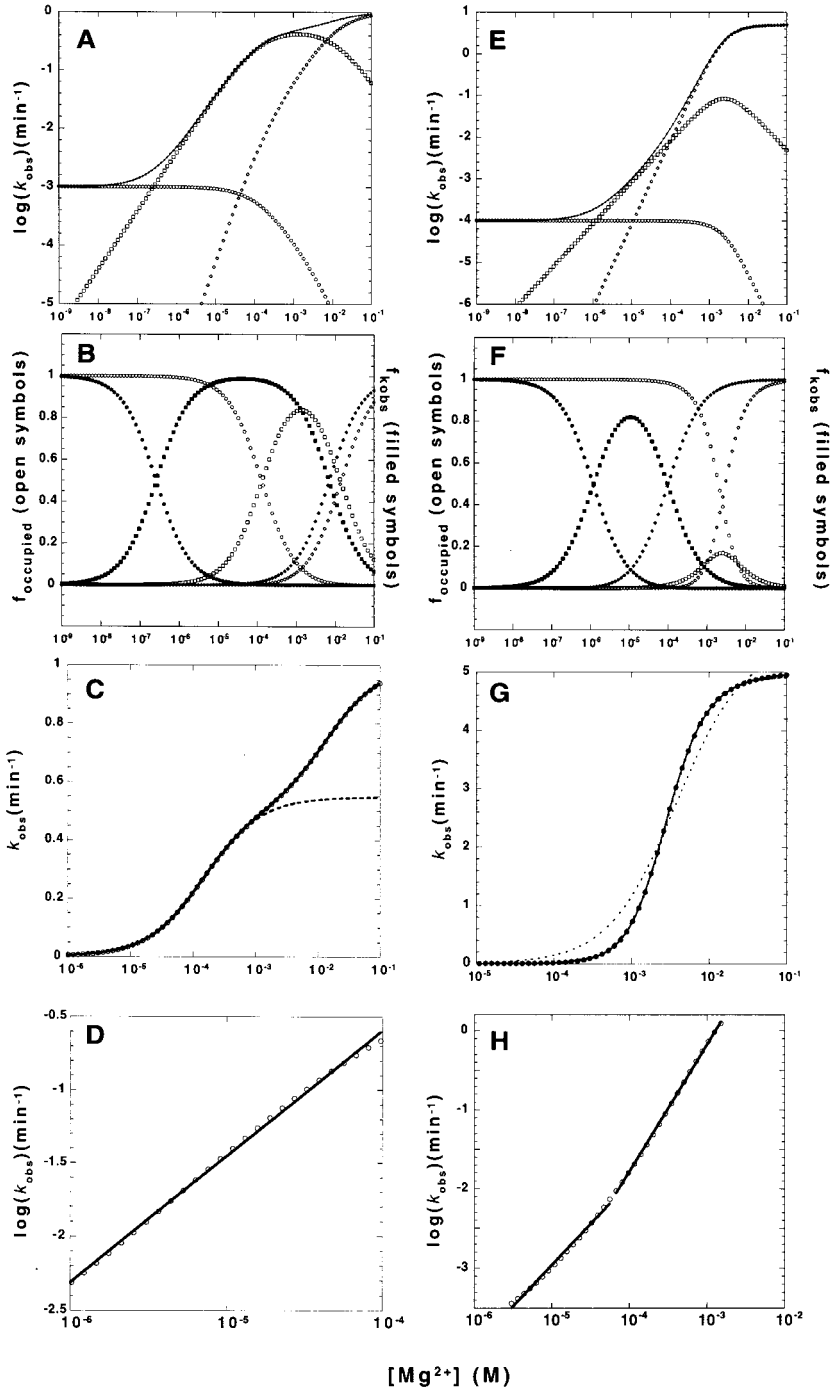

FIGURE 7: Simulations of reactivity−[Mg^{2+}] profiles using estimated values of rate and equilibrium constants at pH 5.0 (A−D) and 8.0 (E−H). Constants for the pH 5.0 simulation were as follows: $k_1 = 0.001$ min^{-1}, $k_2 = 0.5$ min^{-1}, $k_3 = 1.0$ min^{-1}, $K_{d,str} = 0.13$ mM, and $K_{d,cat} = 14$ mM. Constants for the pH 8.0 simulation were as follows: $k_1 = 0.0001$ min^{-1}, $k_2 = 0.05$ min^{-1}, $k_3 = 5$ min^{-1}, $K_{d,str} = 6$ mM, and $K_{d,cat} = 1$ mM. The value of k_2 at pH 8.0 was uncertain, so it was estimated from (k_{obs} at pH 5.0)/10 based on this relationship for k_1 (Figure 5 inset). The values of $K_{d,cat}$ at pH 5.0 and 8.0 were assumed to be similar to those published with no added NaCl (see the text for the modest NaCl dependence of $K_{d,cat}$) (*2*). The value of $K_{d,str}$ at pH 8.0 was assumed to be slightly larger than the K_d from the Hill equation (Table 1). Panels A and E show the log−log dependence of k_{obs} (●) on Mg^{2+} concentration, as well as log(k_1f_1) (○), log(k_2f_2) (□), and log(k_3f_3) (◇), using eqs 9a−9d. Panels B and F show the dependence of fraction occupancy (open symbols) and fraction k_{obs}, defined as k_if_i/k_{obs} (filled symbols), on Mg^{2+} concentration. Circles are for channel 1, squares for channel 2, and diamonds for channel 3. Panels C and G show plots of k_{obs} (nonlogarithmic) vs the higher Mg^{2+} concentrations on a logarithmic axis. Fits to the Hill equation (eq 10) (thick dashed line) and multichannel model (eqs 9a−9d) (solid line) are shown. In panel C, the Hill fit was to the 10^{-6}−10^{-3} M Mg^{2+} points only; fitted parameters were as follows: $k_{max} = 0.55$ min^{-1}, $K_d = 0.15$ mM, and $\alpha_H = 0.96$ (all in good agreement with channel 2 input values). Parameters from the Hill fit at pH 8.0 were as follows: $k_{max} = 4.9$ min^{-1}, $K_d = 2.9$ mM, and $\alpha_H = 1.69$ (indicative of cooperativity in Mg^{2+} binding). For the pH 8.0 simulation, a fit to eq 10 in which α_H was fixed to 1.0 is shown for comparison (thin dashed line). Note that Hill analysis allows the value of k_2 to be obtained at low pH only. Panels D and H show the log−log dependence of k_{obs} on [Mg^{2+}] over an intermediate Mg^{2+} concentration range. At pH 5.0, the slope of the line was 0.86, similar to α_H in panel C. At pH 8.0 and Mg^{2+} concentrations between 3 and ≈56 μM, the slope of the line was 1.03, while at Mg^{2+} concentrations between ≈68 and 1500 μM, the slope of the line was 1.61, similar to α_H in panel G.

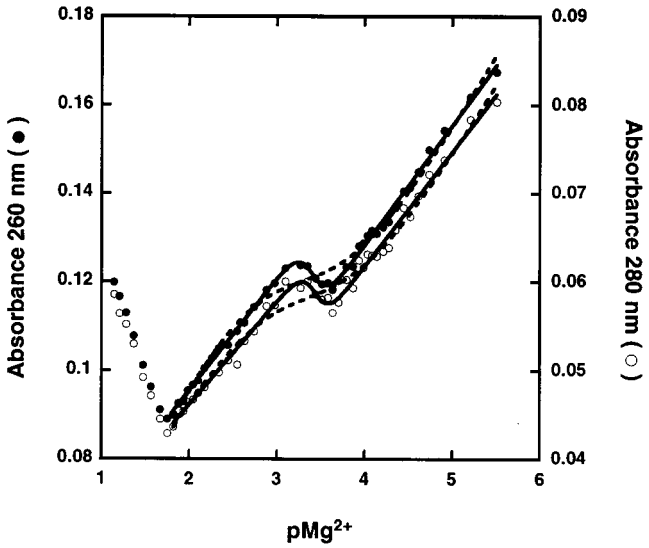

FIGURE 8: Magnesium titrations with absorbance detection. Data are for the self-cleaved G11C ribozyme in 1 M NaCl and 25 mM HEPES (pH 7.0) at 37 °C. Fits to a single-ion model are shown (- - -), as are fits to an *n*-ion model using eq 5 (—). Fits to the 260 nm data (●; left-hand *y*-axis) gave a pK_d of 3.41 ± 0.02 and an α_H of 5.0 ± 0.7, while fits to the 280 nm data (○; right-hand *y*-axis) gave a pK_d of 3.45 ± 0.03 and an α_H of 5.4 ± 1.4 (in good agreement with the 260 nm data). Values and errors for the slopes and intercepts of the upper and lower baselines were reasonable. The nature of the absorbance increase at >10 mM Mg^{2+} is unclear, but could reflect binding of additional metal ions.

divalent ions (*2*), and we show here that qualitatively similar results are obtained in 100 mM Na_2EDTA. These observations strongly suggest that under certain conditions, the HDV ribozyme can cleave without the involvement of divalent metal ions in folding or catalysis. Here we report that the HDV ribozyme uses divalent metal ions to enhance both folding and catalysis. Divalent metal ions appear to contribute ≈3000-fold to folding and catalysis at pH 7.0. This contribution will now be partitioned between folding and catalysis within the context of a multichannel divalent metal ion-dependent model.

Mechanistic Insights from the Divalent Cation-Independent Channels for Self-Cleavage. Experiments carried out in the presence of 1 M NaCl and saturating EDTA revealed a pH profile that was inverted from that observed at high concentrations of Mg^{2+} (Figure 3 and Figure 5 inset). The pH profile was well described by the kinetic model in Scheme 1, which requires two pK_a values for the ribozyme and two channels in the absence of Mg^{2+}. A feature common to the three schemes herein is protonation of C75 in the reactant state, which allows it to act as the general acid. This is based on close positioning (2.7 Å) of N3 of C75 and the leaving group 5′-bridging oxygen of G1 in the crystal structure of the self-cleaved form of the ribozyme (*4*), and observed weaker binding of the catalytic Mg^{2+} ion at lower pH, presumably due to protonation of C75 (*2*). Thus, pK_{a2} in Scheme 1 is assigned to C75. Nevertheless, it is possible to fit the data by assuming that C75 acts as the general base (*1*, *4*), and this possibility has not been definitively ruled out, although it would presumably require that the positioning of C75 and G1 in the crystal structure is accidental.

In 100 mM EDTA, the ribozyme appears to be inhibited by pH values lower than the observed pK_{a1} of 5.6 (Figure 3). It is of interest to consider the possible origin of pK_{a1}

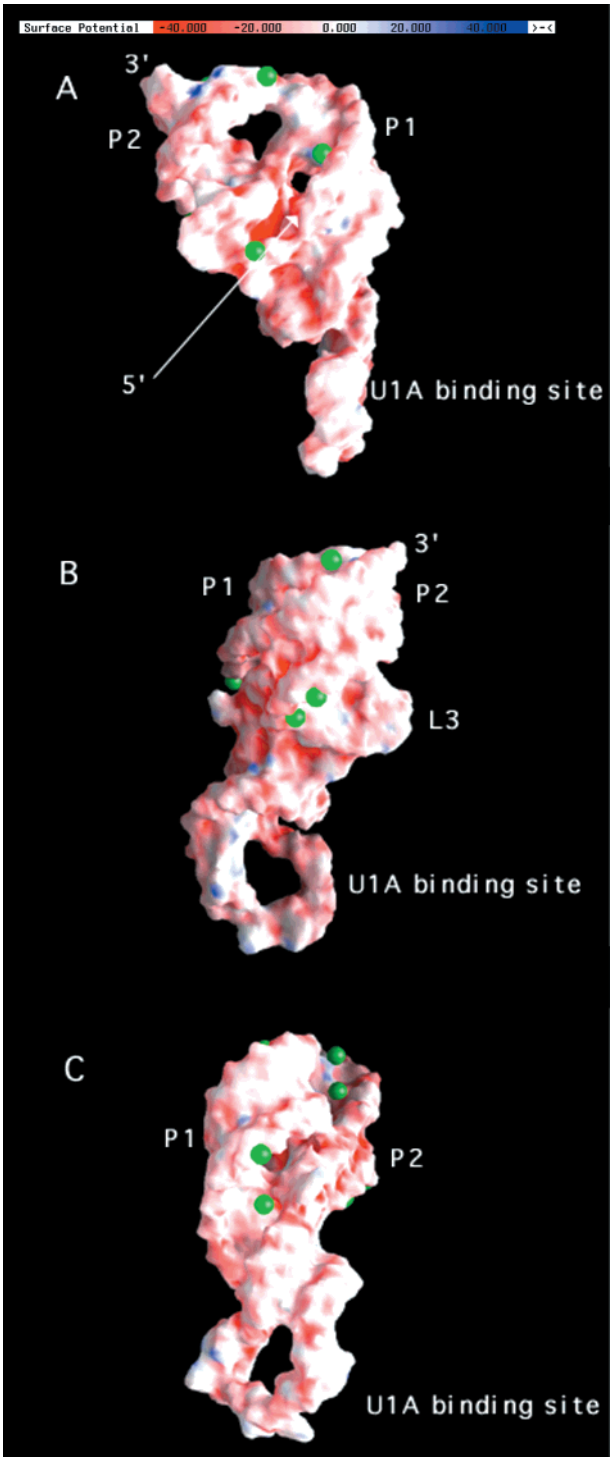

FIGURE 9: Surface potential of the HDV genomic ribozyme. The nine Mg^{2+} ions near the ribozyme are shown, and those near the U1A protein were omitted for clarity. The surface potential is colored according to the scale at the top of the figure. (A) Front view of the catalytic core. The large red channel near the 5′-end has potentials that range from $-30kT/e$ to $-75kT/e$. This may represent the binding site of the catalytic metal ion. (B) View of the molecule after a 120° rotation of the view in panel A about the vertical axis. Again, red patches occur near the center of the molecule in clefts and cavities, as well as near the base of the ribozyme and just above the U1A binding site. (C) View after a 120° rotation of the view in panel B about the vertical axis. Several red patches are visible, including a significant patch just above P1.1, which is part of the same patch in panel A.

(although the identity of this functional group is not critical to the conclusions drawn). This pK_a is unlikely to be related

to disruption of Watson−Crick base pairs since the pK_a values for bases in Watson−Crick pairs are typically shifted away from neutrality (i.e., the pK_a values for C and A are <4.2 and <3.5, respectively; *38*). Another unlikely possibility is that in the absence of $[Mg(OH)]^+$, pK_{a1} (Scheme 1) belongs to a new general base. If under physiological salt conditions C75 acts as the general acid and $[Mg(OH)]^+$ as the general base, then it is unlikely that another RNA atom with a pK_a near neutrality would be found at the active site in a position capable of performing general base catalysis. One plausible origin of the pK_a of 5.8 is a residue involved in formation of an inactive tertiary structure by protonation of a particular base. There is a base quartet in the ribozyme that involves C41 protonated at N3 interacting directly with A43 and G73 (Figure 1C; *5*). In the absence of Mg^{2+} ions, however, this quartet may be prone to misfolding. For example, protonated C41 could interact in a similar fashion with the A43-G74 pair, using the Hoogsteen face of G74. This could disrupt critical contacts between G74 and the core of the ribozyme.

The observed pH profile in Figure 3 is qualitatively similar to published results (*2*), although the rates at low pH were slower in the presence of excess EDTA and the calculated pK_{a2} was shifted toward higher values. The previously reported value for pK_{a2} (Scheme 1) was 5.7 (*2*), which included data to pH 4.5. Fitting of those data to eq 8 rather than to eq 7 and including the pH 4.0 data point gives a value of 5.3 for pK_{a2} (Figure 3). The value of 6.6 at 100 mM EDTA for pK_{a2} (Figure 3) is considerably closer to neutrality and is similar to values observed for C75 at 1−2 mM Mg^{2+} without NaCl (*2*). These data support assignment of pK_{a2} to C75, and suggest that ionic strength is not a strong determinant of a base pK_a value. Measurements of pK_a values for isolated nucleosides and nucleotides are consistent with this interpretation (*39*). Experiments using mutants of the quartet involving C41 in the absence of Mg^{2+} suggest that one of the pK_a values may belong to C41, although no evidence was found for a pK_a for C75 (*31*). However, the minimal kinetic model necessary to fit the data in Figure 3 is surprisingly complex, involving two pK_a values and two Mg^{2+}-free channels (Scheme 1). Contributions of C75 and C41 may depend on the mutants tested and the rates of channels 1′ and 1″ for a given set of conditions. For example, it is possible that if the rates for channel 1′ and 1″ are similar for a given condition, then pK_{a2} could be hidden.

Assessing the Contribution of General Base Catalysis to Rate Acceleration. As the concentration of Mg^{2+} increases, the pH profile of the reaction inverts (Figure 5 inset). This is most readily explained by the filling of the catalytic Mg^{2+} site and participation of the ribozyme-bound $[Mg(OH)]^+$ as the general base. In the presence of 100 mM EDTA, and therefore the absence of $[Mg(OH)]^+$, the question arises as to which species acts as the general base. Because the pH profile of the reaction in Figure 3 is fully described by the kinetic model in Scheme 1, there is no need to invoke a general base with a pK_{a3} of >4.5, the lowest pH measured in the experiments. One candidate for the general base under such conditions is solvent water. Although the pK_a of the conjugate acid of water is only −1.7, the concentration of water is 55 M. Indeed, Brønsted analysis has implicated water as the general base in the H12A mutant of ribonuclease A, where H12 serves as the general base in the wild-type enzyme (*40*). The rate−pH profile of the ribozyme observed at high pH (>8) is most readily explained by involvement of hydroxide ion in the reaction (Scheme 1, channel 1″). Modeling of a hydroxide ion-catalyzed channel into Scheme 1 provides a good fit to the data and explains the plateau of the rate−pH profile at high pH as being due to a change in the major channel for cleavage from channel 1′ to channel 1″.

If water is reacting as the general base via channel 1′, then the second-order rate constant for water in 100 mM Na_2-EDTA is 6.2×10^{-5} M^{-1} min^{-1} (0.0034 min^{-1}/55 M; Figure 3). For hydroxide ion in channel 1″, the second-order rate constant is 2.8×10^3 M^{-1} min^{-1} (Figure 3), ($\approx 4.5 \times 10^7$)-fold faster than water. This leads to a Brønsted coefficient, β, for general base catalysis of 0.44 ± 0.05 [$=\log 4.5 \times 10^7/(15.7 - -1.7)$] (see Methods for an estimation of error in β). Note that any poor folding of the ribozyme in the absence of divalent metal ions (see the next section) should affect both the solvent- and hydroxide-catalyzed reactions equally, and thus cancel. The β value from this simple model is similar to typical values of 0.5 for proton transfers between oxygen and nitrogen (*41*), and similar to the β value for general base catalysis by RNase A (*40*). A β value of 0.44 suggests that the charge is nearly equally shared between the acceptor and donor atoms in the transition state. This analysis supports the conclusion that general base catalysis is important to the mechanism of self-cleavage of the HDV ribozyme.

Recently, a Brønsted analysis was carried out by Shih and Been for C76 of the antigenomic HDV ribozyme (*3*). They made a C76 deletion and rescued cleavage activity with a series of small molecules, including imidazole derivatives. Brønsted analysis gave a β of 0.51 (or an α of 0.49) and further implicated C75 in proton transfer (*3*). Together with our results here, the data suggest that C75 and hydroxide ion, metal-bound or from solvent (see the next section), may act as the general acid and general (or specific) base, respectively. This would be similar to the mechanism of RNase A, wherein His119 and His12 act as the general acid and base with α and β values of approximately 0.5 each, respectively (*40*). Shih and Been carried out a proton inventory of the reaction, and found an inventory of one proton transfer in the rate-limiting step (*3*). Proton inventories of two have been observed for RNase A (*42*). The number of protons detected in the inventory on HDV may be dependent on different solution conditions (S. Nakano and P. C. Bevilacqua, unpublished experiments).

Assessing the Contribution of Mg^{2+} Ions to Rate Acceleration. The data presented herein are consistent with two classes of divalent metal ions, structural and catalytic. The data were fit to a kinetic model involving three major channels for cleavage (Scheme 2). A more complicated model involving four major channels and random binding of structural and catalytic metal ions was also considered. However, such a model would not predict cooperative binding of metal ions at high pH, under which conditions the catalytic metal ion binds tighter than the structural metal ions. Thus, the model involving ordered binding of structural and catalytic metal ions appears to be the simplest model consistent with the data, and at least one of the more complicated models appears to be less likely.

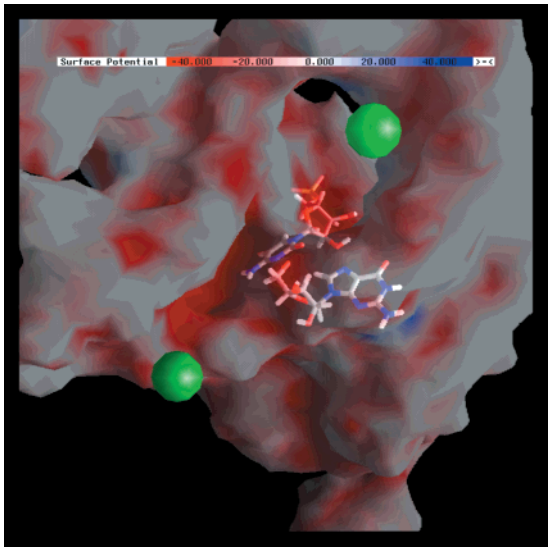

FIGURE 10: Positioning of C75 in the negative cleft at the active site. G1 and C75 are shown in stick representation with atoms colored as follows: hydrogen in white, carbon in gray, oxygen in red, nitrogen in blue, and phosphorus in yellow. The surface potential is colored according to the scale at the top of the figure. The surface was set to 50% transparency using GRASP (*28*), to allow visualization "through" the surface. Colors shaded on bonds represent potentials in those areas. The exocyclic amine of C75 is positioned in the negative cleft with a local potential of approximately $-40kT/e$. This value may be more negative if the scissile phosphate is nearby. Negative potential near N4 could serve to stabilize protonation of N3 assuming significant electron donation from N4. The Mg^{2+} ion in the lower left part of the figure is 11.5 Å from the 5′-oxygen of G1. The dimensions of the negative cleft are approximately 14.5 Å × 3.5 Å with a depth of approximately 15.5 Å.

The absorbance titrations suggest that there are approximately five divalent metal ions that bind to the self-cleaved ribozyme and induce a new conformation (Figure 8). Observation of a slope of 1 rather than 5 in the log k_{obs} versus log[Mg^{2+}] plots (Figure 5) may reflect one of these structural ions being especially important to the active conformation. This would be similar to the phenomenon described in the comparison of experimental and simulated self-cleavage data at high pH where cooperative metal ion binding occurs but only one metal ion is observed at low Mg^{2+} concentrations in the rate profile (Figures 6 and 7). Currently, it is unclear where these metal ions bind. Possible binding sites are suggested by the NLPB calculations, by the crystal structure (*5*) (Figures 9 and 10), and by peripheral metal ions mapped in the ribozyme (*43*). These sites are distributed throughout the ribozyme, but the current data do not indicate which specific sites are filled in the experiments performed herein.

Binding of multiple divalent metal ions to RNAs with compact tertiary structures has been observed previously (*33*). For example, tRNA, which is about the same size as the HDV ribozyme, typically has been found to have four to six site-bound Mg^{2+} ions using NMR, ESR, calorimetry, equilibrium dialysis, and equilibrium fluorescence titration (*33*). In fact, K_d values for Mg^{2+} ions site-bound to tRNA are only 10−30-fold tighter than those found in this study, and the tRNA studies were carried out at 10−30-fold lower NaCl concentrations (*33*). (Inhibition of site binding of Mg^{2+} by NaCl is expected purely on the basis of electrostatic effects.) This suggests that the affinities of Mg^{2+} binding to tRNA and to the HDV ribozyme may be similar.

The structural divalent metal ion binds tighter at low pH, while the catalytic divalent metal ion binds tighter at high pH (Figure 5, Table 1). Tighter binding of the structural metal ion at low pH may be related to the pH-dependent formation of a quartet involving a protonated C41 (S. Nakano and P. C. Bevilacqua, unpublished experiments), and tighter binding of the catalytic metal ion at high pH appears to be due to electrostatic repulsion with the protonated C75 in the ground state (*2*). Failure to observe binding of the structural metal ions at low NaCl concentrations in a previous study (*2*) may reflect enhanced binding of structural metal ions under those conditions such that they bind with a K_d that is lower than the concentration of Mg^{2+} examined in that study (≈20−70 μM). Overall, the data suggest that NaCl competes effectively for binding of the structural metal ions, but poorly for the catalytic metal ion.

The contribution of Mg^{2+} ions to k_{obs} at pH 7.0 can be estimated to be ≈3000-fold based on the rate in 1 M NaCl with and without saturating 10 mM $MgCl_2$ (=4 min^{-1}/0.0013 min^{-1}) (see the Figure 5 inset). The contribution of Mg^{2+} ions can be to folding or chemistry. The data are consistent with a multichannel model for self-cleavage, as described above and shown in Scheme 2. However, the data are also consistent with Scheme 3, which differs from Scheme 2 by having only the correctly folded ribozyme (R) in rapid equilibrium with the partially folded ribozyme (R′). Under these conditions, k_2 and k_1 are related by eq 11, which has the limit of $k_2 = k_1K_{unfold}$ for large K_{unfold} values. According to Scheme 3, channels 1 and 2 cleave with the same intrinsic rate constant, k_2, but k_2 is not observed for channel 1 because the ribozyme spends most of its time in a partially folded state. This model is attractive since channels 1 and 2 have the same "inverted" pH profiles, suggesting that $[Mg(OH)]^+$ is not participating in the chemical step in either channel, and that the rate constants for chemistry should be similar for both channels. If the observed rate constants for channels 1 and 2 are related by eq 11, then the K_d for the structural Mg^{2+} ion should be affected by K_{unfold} according to eq 12, which has the limit of $K'_{d,str} = K_{d,str}/K_{unfold}$ for large K_{unfold} values, where $K'_{d,str}$ is the intrinsic binding constant for Mg^{2+} binding to a fully formed binding site. This model suggests that the structural Mg^{2+} ion(s) binds weaker with an observed binding constant, $K_{d,str}$, because it has to spend part of its free energy of binding in inducing the correct fold of ribozyme. Evidence that a folding transition is occurring in this process was obtained in part from the change in absorbance upon Mg^{2+} addition (Figure 8). Perhaps the regions of high negative potential, including the active site, fold fully only in the presence of divalent metal ions even though 1 M NaCl is present (Figures 9 and 10).

The value of K_{unfold} can be estimated from k_2 and k_1. An estimate of k_2 was obtained from the low-pH Mg^{2+} titrations, with a k_2 of 0.5 min^{-1} at pH 5.0 (Figures 6 and 7). An estimate of k_1 was obtained from k_{solv} (Figure 3) as 0.004 min^{-1}, and these values provide a K_{unfold} of ≈125. This value of K_{unfold} is used at pH 7 since k_{OH^-} does not appear to contribute substantially at pH 7 (Figure 3). The observed K_d for Mg^{2+} at pH 7.0 and 1 M NaCl is 2.2 mM (Table 1). The above analysis suggests that the intrinsic value of this Mg^{2+} binding is ≈18 μM (=2.2 mM/125) in the presence of 1 M

NaCl at pH 7.0.

If Mg^{2+} ions contribute ≈125-fold in going from channel 1 to 2 (Scheme 3), then the extra contribution to k_{obs} in going from channel 2 to channel 3 is ≈25-fold (=3000/125) at pH 7.0. This value is similar to the difference in rate at 0.1 and 10 mM Mg^{2+}, where the curve undergoes inversion at pH 7.0 (Figure 5 inset). Thus, the actual contribution of Mg^{2+} to the chemical step appears to be modest. The contribution of Mg^{2+} to catalysis can be treated with the following Brønsted analysis. This analysis assumes that the concentrations of saturating Mg^{2+} and of water in the absence of Mg^{2+} are similar at the active site, as was done for the concentrations of histidine versus water in the H12A mutant of RNase A (*40*). The rate acceleration determined from the Brønsted equation is $k_3/k_2 = [K_a^{H_3O^+}/K_a^{Mg(H_2O)_6}]^{\beta} \times 10^{pK_{a,C75}-11.4}$, where $K_a^{H_3O^+} = 10^{1.7}$, $K_a^{Mg(H_2O)_6} = 10^{-11.4}$, $\beta = 0.44$, $pK_{a,C75} = 5.86$, and the $10^{pK_{a,C75}-11.4}$ term accounts for the fraction of Mg^{2+} not in the functional hydroxide form. The value for $pK_{a,C75}$ in 10 mM Mg^{2+} and 1 M NaCl is from a fit to the Figure 5 inset (data not shown), and this value is similar to that without NaCl (*2*). Thus, the Brønsted analysis predicts $k_3/k_2 = 10^{(13.1)(0.44)}10^{-5.54} = 1.7$. This value is only 15-fold different from the k_3/k_2 ratio of 25 extracted from analysis of the multichannel model. (The 15-fold discrepancy is small and may be due to errors in k_2, k_3, β, or $pK_{a,C75}$, a higher-than-assumed effective concentration of saturating Mg^{2+}, or to contributions from the catalytic Mg^{2+} ion in charge stabilization or folding.) This analysis suggests that even though the pK_a of $[Mg(OH)]^+$ is 13.1 units greater than that of solvent water, it is compromised in its ability to abstract a proton because it is largely in the nonfunctional fully hydrated form at neutral pH and because $\beta < 1$. Consistent with this interpretation, there appears to be little involvement of the catalytic metal ion at pH 5.0 and 10 mM Mg^{2+} based upon the leveling off of k_{obs} between pH 5 and 4 (Figure 5 inset).

The poor reactivity of $[Mg(OH)]^+$ is consistent with the optimal pK_a for a general acid−base catalyst being neutrality, as in C75 in the HDV ribozyme and His12 and His119 in RNase A (*40*). Lack of a general base with a pK_a near neutrality for the HDV ribozyme can account for its 10^5-fold slower rate of cleavage compared to RNase A (*2*). Nevertheless, there does not appear to be any reason a priori why an RNA enzyme could not have both its general acid and general base possess pK_a values of neutrality and so react at a rate similar to that of RNase A. Under saturating Mg^{2+} conditions, the HDV ribozyme studied herein reacts with a half-life of <10 s, and this may be sufficiently fast that there is no selective pressure for this single-turnover ribozyme to react any faster. One possibility is that RNA folding events, especially resolving of misfolded structures (ref *10* and unpublished experiments of D. M. Chadalavada and P. C. Bevilacqua), are rate-limiting during rolling circle replication.

The pH profile at 10 mM Mg^{2+} is consistent with $[Mg(OH)]^+$ acting as the general base, as previously discussed (*2*), although a related model is now considered. The above analysis in saturating EDTA suggests that hydroxide ion may act as a specific base at high pH in the absence of a catalytic contribution from Mg^{2+} ions. The pH profile observed at 10 mM Mg^{2+} is also consistent with hydroxide ion from solvent acting as a specific base and Mg^{2+} at the active site acting to stabilize negative charge. An electrostatic role for a catalytic divalent metal ion was also suggested from analysis of the crystal structure of the ribozyme (*5*). Currently, we are unable to conclude whether the active hydroxide species is originating from solvent, the bound divalent metal ion, or both; furthermore, the major contribution may be dependent on the pK_a of the metal ion and may switch with pH. However, competitive inhibition by $[Co(NH_3)_6]^{3+}$ would seem to argue that a hydrated divalent metal hydroxide is important under certain conditions (*2*).

The contribution of the RNA bases to the reaction can also be partitioned into catalytic and folding contributions. Substitution of C75 and C76 with A led to an ≈300-fold decrease in cleavage rate for the genomic ribozyme (*2*), and a 4000-fold decrease for the antigenomic ribozyme (*1*). Brønsted analysis of the contributions of A and C suggests that the effect of the mutation on proton transfer should be small because the pK_a values of the nucleotides are similar, as are the pK_a values of the wild-type and mutant ribozymes (*2*). The large observed effects suggest that C75 may also have important roles in folding, especially in the precursor form of the ribozyme. In addition, completion of the self-cleavage reactions for the C75A mutant was strongly affected by pH and Mg^{2+} concentration unlike the C75 ribozyme (data not shown), consistent with the role of C75 in ribozyme folding. The inability to detect any reaction with C75U/C76U mutants also supports a role for C75 in folding (*1*, *2*), although this is also consistent with a potential general base role for C75 since the N3 pK_a of U is >9. Apparently, C75 plays important roles in both catalysis and folding of the ribozyme.

Surface potential calculations revealed an extensive negative channel near C75 and the 5′-hydroxyl of G1 (Figure 10). In the crystal structure, a well-defined metal ion was not observed in this channel, although weak electron density was seen which might represent low occupancy by a divalent metal ion (*5*). Also, well-resolved divalent metal ions were found near either end of the cleft, with one ion within 11.5 Å of the O5′ of G1 (Figure 10). The positioning of the scissile phosphate in the reactive conformation is currently unknown. However, it should be near the 5′-hydroxyl of G1, and this might serve to further increase the negative potential at the active site. This increase could aid binding of a new ion or repositioning of one of the nearby ions, allowing participation in catalysis. A large negative potential might also stabilize development of a positive charge on C75 and help shift its pK_a toward neutrality. In particular, N4 of C75 is found deep in the negative cleft (Figure 10). Protonation of N3 could be stabilized by electron donation from N4, which could in turn be stabilized by this negative potential.

Summary. In the mechanisms of phosphodiester bond cleavage by four small ribozymes, divalent metal ions can be removed while retaining catalytic ability. Remaining catalytic ability is within approximately 10−20-fold of the wild-type activity for the hammerhead and hairpin ribozymes (*9*, *35*, *36*, *44*−*46*). The data presented herein can be described by a multichannel mechanism in which the HDV ribozyme cleaves by the fastest channel available to it under a given set of solution conditions. Dissection of structural and catalytic roles of Mg^{2+} ions suggests that Mg^{2+} ions contribute approximately 125-fold to folding and 25-fold to catalysis. The modest contribution of Mg^{2+} to catalysis can be described by a Brønsted analysis, which suggests that

water and hydroxide ion can act as bases with little penalty. In contrast, C75 contributes more to cleavage than expected from a Brønsted analysis, suggesting this residue may also be important in attaining the proper tertiary fold of the ribozyme.

ACKNOWLEDGMENT

We thank Juliette Lecomte and members of the Bevilacqua laboratory for critical comments on the manuscript. We also thank David Draper and Ross Shiman for helpful conversations on working with Chelex resin and for suggesting NLPB calculations, and Michael Been for helpful discussions and comments on the manuscript.

REFERENCES

1. Perrotta, A. T., Shih, I., and Been, M. D. (1999) *Science 286*, 123−126.
2. Nakano, S., Chadalavada, D. M., and Bevilacqua, P. C. (2000) *Science 287*, 1493−1497.
3. Shih, I. H., and Been, M. D. (2001) *Proc. Natl. Acad. Sci. U.S.A. 98*, 1489−1494.
4. Ferre-D'Amare, A. R., Zhou, K., and Doudna, J. A. (1998) *Nature 395*, 567−574.
5. Ferre-D'Amare, A. R., and Doudna, J. A. (2000) *J. Mol. Biol. 295*, 541−556.
6. Dahm, S. C., Derrick, W. B., and Uhlenbeck, O. C. (1993) *Biochemistry 32*, 13040−13045.
7. Shih, I. H., and Been, M. D. (1999) *RNA 5*, 1140−1148.
8. da Silva, F., and Williams, R. J. P. (1993) *The Biological Chemistry of the Elements*, Oxford University Press, Oxford, U.K.
9. Murray, J. B., Seyhan, A. A., Walter, N. G., Burke, J. M., and Scott, W. G. (1998) *Chem. Biol. 5*, 587−595.
10. Chadalavada, D. M., Knudsen, S. M., Nakano, S., and Bevilacqua, P. C. (2000) *J. Mol. Biol. 301*, 349−367.
11. Perrin, D. D., and Dempsey, B. (1974) in *Buffers for pH and Metal Ion Control*, pp 4−23, Chapman and Hall, London.
12. Holmquist, B. (1988) *Methods Enzymol. 158*, 6−12.
13. Kennedy, J. H. (1984) in *Analytical Chemistry Principles*, pp 283−287, Harcourt Brace Jovanovich, San Diego.
14. Martel, A. E., and Smith, R. M. (1974) in *Critical Stability Constants*, Vol. 1, pp 204−211, Plenum Press, New York.
15. Baker, J. O. (1988) *Methods Enzymol. 158*, 33−55.
16. Cantor, C. R., and Schimmel, P. R. (1980) in *Biophysical Chemistry*, pp 863−866, W. H. Freeman and Co., New York.
17. Jencks, W. P. (1987) in *Catalysis in Chemistry and Enzymology*, pp 163−242, Dover Publications, New York.
18. Sharp, K. A., Friedman, R. A., Misra, V., Hecht, J., and Honig, B. (1995) *Biopolymers 36*, 245−262.
19. Chen, S. W., and Honig, B. (1997) *J. Phys. Chem. B 101*, 9113−9118.
20. Chin, K., Sharp, K. A., Honig, B., and Pyle, A. M. (1999) *Nat. Struct. Biol. 6*, 1055−1061.
21. Misra, V. K., and Draper, D. E. (2000) *J. Mol. Biol. 299*, 813−825.
22. Maderia, M., Hunsicker, L. M., and DeRose, V. J. (2000) *Biochemistry 39*, 12113−12120.
23. Correll, C. C., Freeborn, B., Moore, P. B., and Steitz, T. A. (1997) *Cell 91*, 705−712.
24. Cate, J. H., and Doudna, J. A. (1996) *Structure 4*, 1221−1229.
25. Word, J. M., Lovell, S. C., Richardson, J. S., and Richardson, D. C. (1999) *J. Mol. Biol. 285*, 1735−1747.
26. Gilson, M. K., Sharp, K. A., and Honig, B. (1987) *J. Comput. Chem. 9*, 327−335.
27. Gilson, M. K., and Honig, B. (1988) *Proteins 4*, 7−18.
28. Nicholls, A., Sharp, K. A., and Honig, B. (1991) *Proteins 11*, 281−296.
29. Suh, Y. A., Kumar, P. K., Taira, K., and Nishikawa, S. (1993) *Nucleic Acids Res. 21*, 3277−3280.
30. Martel, A. E., and Smith, R. M. (1974) in *Critical Stability Constants*, Vol. 3, pp 161−164, Plenum Press, New York.
31. Wadkins, T. S., Shih, I., Perrotta, A. T., and Been, M. D. (2001) *J. Mol. Biol. 305*, 1045−1055.
32. Jencks, W. P. (1975) *Adv. Enzymol. 43*, 219−410.
33. Misra, V. K., and Draper, D. E. (1998) *Biopolymers 48*, 113−135.
34. Misra, V. K., and Draper, D. E. (1999) *J. Mol. Biol. 294*, 1135−1147.
35. Curtis, E. A., and Bartel, D. P. (2001) *RNA 7*, 546−552.
36. O'Rear, J. L., Wang, S., Feig, A. L., Beigelman, L., Uhlenbeck, O. C., and Herschlag, D. (2001) *RNA 7*, 537−545.
37. Rupert, P. B., and Ferre-D'Amare, A. R. (2001) *Nature 410*, 780−786.
38. Legault, P., and Pardi, A. (1997) *J. Am. Chem. Soc. 119*, 6621−6628.
39. Izatt, R. M., Christensen, J. J., and Rytting, J. H. (1971) *Chem. Rev. 71*, 439−481.
40. Thompson, J. E., and Raines, R. T. (1994) *J. Am. Chem. Soc. 116*, 5467−5468.
41. Jencks, W. P. (1985) *Chem. Rev. 85*, 511−527.
42. Matta, M. S., and Vo, D. T. (1986) *J. Am. Chem. Soc. 108*, 5316−5318.
43. Lafontaine, D. A., Ananvoranish, S., and Perreault, J.-P. (1999) *Nucleic Acids Res. 27*, 3236−3243.
44. Hampel, A., and Cowan, J. A. (1997) *Chem. Biol. 4*, 513−517.
45. Nesbitt, S., Hegg, L. A., and Fedor, M. J. (1997) *Chem. Biol. 4*, 619−630.
46. Young, K. J., Gill, F., and Grasby, J. A. (1997) *Nucleic Acids Res. 25*, 3760−3766.

BI011253N